Nonlinear optical properties of glass

Marc Dussauze, Thierry Cardinal

Nonlinear Optical Properties of Glass

Marc Dussauze, Thierry Cardinal

Abstract:

Numerous innovations in photonics were realized on the base of nonlinear optical properties and notably in information technologies. To take advantage of nonlinear optical properties of glass, multi-disciplinary research efforts were necessary combining optics, glass chemistry, material science as well as development of optical or electrical polarizations processes. This chapter addresses both fundamental aspects of the nonlinear optical responses, but also the exploitation of nonlinear optical phenomena in glassy material. It starts by a general introduction on nonlinear optical phenomena and concepts. Then, the specific cases of second and third optical responses in glasses are treated separately and described in details as a function of the corresponding optical phenomena, the different glass families and the applications.

Authors informations

Dr. Marc Dussauze, 39, Chargé de recherche CNRS, Université de Bordeaux, France

Marc Dussauze is currently a CNRS researcher at the Institute of Molecular Science (ISM) from the University of Bordeaux. He is specialist in glass chemistry, nonlinear optics as well as in structural characterizations by vibrational spectroscopy. His investigations are mainly related to the development of optical or electrical polarization processes to manage chemical and optical (linear and nonlinear) properties of glassy materials at different scale.

He received a PhD in physical-chemistry of condensed matter from the University of Bordeaux in 2005. Prior to enter the CNRS in 2009, Marc Dussauze was a postdoctoral fellow at the National Hellenic Research Foundation of Athens, Greece. He received the CNRS bronze medal in 2016.

Dr. Thierry Cardinal, 47, CNRS, Director of Research at ICMCB, University of Bordeaux.

He has co-authored about 120 publications in peer reviewed journals Thierry Cardinal is director of the LIA LUMAQ (International Associate Laboratory) on photonics and Lasers between University of Bordeaux, Laval University and INRS in Canada.

He is specialized in new inorganic materials for photonics and laser structuring. He has investigated nonlinear optical properties in glass (Kerr effect and Raman Gain). He has demonstrated the advantage of noble ion containing glass for implementing, using direct femtosecond laser writing process, local luminescence and second order nonlinearity.

1. General introduction on nonlinear optical properties

Nonlinear optical (NLO) properties investigations in glass are intimately related to the discovery of Lasers [1]. At the early age of lasers, most of the investigations were devoted to crystals and especially to non-centrosymmetric materials such as Quartz, $LiNbO_3$, $KTiOPO_4$ (KDP), and α-BaB_2O_4 (BBO).[2] Numerous innovations in photonics were realized, such as frequency conversion, which allows expansion of the range of accessible wavelength by taking advantage of second and third harmonic generation or frequency sum or difference using only one or few monochromatic laser lines thanks to high power laser material interaction. Glasses, due to their isotropic nature, do not exhibit second order nonlinearity: second harmonic generation (SHG) or electro optic effect (Pockels effect). Then, in contrast to the field of crystalline compounds for which the NLO properties have led to rapid scientific and technological revolution, the NLO phenomena in glass have been considered more like a constraint for practical use. Indeed, the interest in NLO properties of glass appears with the development of high power lasers and the growth of the optical information transmission in the telecom sector. The main objectives were to investigate the light propagation and the perturbation of the wave front while limiting the detrimental effects of NLO phenomena in waveguides where high density of photon occurs. For instance, the Kerr effect (third order nonlinearity), at the origin for a change in the refractive index with the laser intensity, is responsible for a spectacular self-focusing phenomenon due to the formation of a photo-induced lens directly linked to the intensity-spatial profile of the beam. This lensing could result, at worst, to an optical breakdown or a to an alteration of the wave front propagation.

Such effects are still of importance for laser ignition facilities such as the MegaJoule laser (LMJ) in France or the National Ignition Facility in the USA. In the telecom sector, the issue was raised by the current use of small fiber core diameter of a few micrometers in which the power density of the optical signal over a long distance can give rise to prolonged laser material

interaction. In that case again, the choice has been made to select materials exhibiting the lowest NLO effects to prevent any optical signal distortion. In the last 25 years, NLO properties have been exploited in optical fiber to generate soliton wave propagation to minimise the signal attenuation during its propagation.

In the scientific community, it is mainly in the late 1980s that articles mentioning the opportunity of NLO properties in inorganic glass began to appear.[3] [4] Once again, the interest is related to the development of novel light source able to deliver energy in a short time and able to generate a high electric field in matter. These short-pulse lasers brought to the laboratories the possibility to access to electric field (10^{10} V/m) on the order of that between outer-most electrons and the atom. Rapidly the field became important and numerous articles have been published on the investigation of NLO properties of glasses. Indeed, the short-pulse laser has developed the interest in nonlinear optical properties of glasses such as ultrafast intensity–dependent index, third harmonic generation, Stimulated Raman, second harmonic generation, and multiphoton absorption.

2. The concept of polarization at the microscopic scale

To describe the nonlinear optical response of a medium, we will first introduce the concept of polarization. Light is an electromagnetic wave described by an electric (E) and a magnetic (B) field. The direction of light propagation is perpendicular to these two fields and Maxwell's equations permit a full description of its propagatation. On dielectric medium (such as glasses), the magnetic field part of light can be generally neglected. The electric field can be written as:

$$E(r,t) = E_0(e^{(ik.r-i\omega t)}) \quad (1)$$

With ω being the angular frequencyof the electromagnetic field also equals to 2πν (ν being the frequency), $\omega.t$ a time-dependent phase term and $k.r$ a space-dependent phase term. k is the

wave vector that indicates the direction of light propagation, it is equal to $2\pi n/\lambda$ (n being the refractive index, λ being the wavelength), r is the position vector.

Matter can be described as an association of a positive point charges (core) surrounded by a cloud of negative charges (electrons) which, in a first approximation, is described as a dipole characterized by its dipole moment M a vector describing the separation of the positive and negative charges. Once an electric field is applied to the medium, the core tends to move in the direction of the field and the electrons in the opposite direction. Due to their lower mass, the electrons movement is much more significant leading to a faster response. The deformation of the electrons cloud cause a charge separationcharacterized by a microscopic dipole moments μ. Under illumination, the microscopic dipole moments oscillate at the frequency of the incident electric field. Dielectric dipole moments at the microscopic scale results in a macroscopic polarization of the medium described as the sum of all the microscopic dipoles. If the illumination is of a high intensity, i.e. of the order of the atomic cohesion forces, the cloud of electrons oscillate with a higher amplitude deviating from a harmonic oscillation. The resulting nonlinear polarization is described in a power series as a function of the local electric field. The induced dipole moment at the microscopic scale can be written in a first approximation as:

$$\begin{aligned} \mu_{ind}(\omega) = {} & \mu^{(1)}(\omega) + \mu^{(2)}(\omega) + \mu^{(3)}(\omega) + \cdots \\ & = \alpha F(\omega) + \beta F(\omega)F(\omega) + \gamma F(\omega)F(\omega)F(\omega) \\ & + \cdots \end{aligned} \qquad (2)$$

With α the molecular first order polarizability or linear polarizability while β and γ are respectively the second and third order polarizability terms which described the nonlinear induced polarization and F the local field . It is important to note that because of interactions between dipoles at the microscopic scale, the local field *F* is not equal to the electric field E of the incident light. A local field factor (f) is thus necessary to account for interactions between

neighboring dipoles. A common form of the local field factor is given by the Lorentz-Lorenz approximation and takes into account these interactions.[5] The local field F can be written as

$$\vec{F} = f\vec{E} \qquad (3)$$

3. The concept of polarization at the macroscopic scale

The macroscopic polarization, as a function of time and space, of a material under the influence of an applied electric field can be described in terms of a power series of the field:

$$\vec{P}_i(\vec{r};t) = \vec{P}_i^{(0)}(\vec{r};t) + \vec{P}_i^{(1)}(\vec{r};t) + \vec{P}_i^{(2)}(\vec{r};t) + ... + \vec{P}_i^{(n)}(\vec{r};t) + ... \qquad (4)$$

where $\vec{P}_i^{(0)}(\vec{r};t)$ represents the static polarization (null in glass), $\vec{P}_i^{(1)}(\vec{r};t)$ is linear in the field, $\vec{P}_i^{(2)}(\vec{r};t)$ is quadratic, and so on. The most general expression for the linear polarization, with the assumptions of *homogeneity* of the material and *invariance by time translation* and the *causality principle*

$$\vec{P}_i^{(1)}(\vec{r};t) = \varepsilon_0 \int_0^t R_{ij}^{(1)}(\vec{r};t-t_1)\vec{E}_j(\vec{r};t_1)dt_1 = \varepsilon_0 R_{ij}^{(1)}(t) \otimes \vec{E}_j(t) \qquad (5)$$

Since this last expression is a convolution product, it is natural to pass into the frequency domain, where the linear polarization is a simple product

$$\vec{P}_i(\omega) = \varepsilon_0 \chi_{ij}^{(1)}(-\omega_\sigma;\omega)\vec{E}_j(\omega) \qquad (6)$$

where $\chi_{ij}^{(1)}(-\omega_\sigma;\omega) = \int_{-\infty}^{+\infty} R_{ij}^{(1)}(t_1)\exp(i\omega t_1)dt_1$ is the first-order susceptibility of the material, a second-rank tensor. In these equations $\omega_\sigma = \omega$.

With the same assumptions as in the previous paragraph (homogeneity, time invariance, locality and causality), the quadratic, cubic and higher order polarizations are expressed as

$$\vec{P}_i^{(n)}(\vec{r};t) = \varepsilon_0 \int_0^t \int_0^t ... \int_0^t R_{ij...\eta}^{(n)}(\vec{r};t-t_1,t-t_2,...,t-t_n)\vec{E}_j(\vec{r};t_1).\vec{E}_k(\vec{r};t_2)...\vec{E}_\eta(\vec{r};t_n)dt_1dt_2...dt_n \quad (7)$$

where $Rij...\eta^{(n)}$ is the total response function of the material taking into account the time response. As we will see, later the time response of the material can have an important impact on the NLO properties. $\chi^{(n)}$ can be defined as the n^{th}-order susceptibility obtained by the Fourier transform of the response function of the material

$$\chi_{ij...\eta}^{(n)}(-\omega_\sigma;\omega_1,\omega_2,...,\omega_n) = \int_{-\infty}^{+\infty} R_{ij...\eta}^{(n)}(t_1,t_2,...,t_n)\exp\left[i(\omega_1 t_1 + \omega_2 t_2 + ... + \omega_n t_n)\right]dt_1dt_2...dt_n \quad (8)$$

where $R_{ij...\eta}^{(n)}$ is an $(n+1)$-rank tensor denoted as the n^{th}-order response function of the material.

By expressing the response functions and the electric fields with their respective Fourier transforms, the equations and can be rewritten as

$$\vec{P}_i^{(2)}(\vec{r};t) = \frac{\varepsilon_0}{(2\pi)^2}\int_{-\infty}^{+\infty}\int_{-\infty}^{+\infty}\chi_{ijk}^{(2)}(-\omega_\sigma;\omega_1,\omega_2)\vec{E}_j(\vec{r};\omega_1).\vec{E}_k(\vec{r};\omega_2) \times \exp\left[-i(\omega_1+\omega_2)t\right]d\omega_1 d\omega_2 \quad (9)$$

$$\vec{P}_i^{(3)}(\vec{r};t) = \frac{\varepsilon_0}{(2\pi)^3}\int_{-\infty}^{+\infty}\int_{-\infty}^{+\infty}\int_{-\infty}^{+\infty}\chi_{ijkl}^{(3)}(-\omega_\sigma;\omega_1,\omega_2,\omega_3)\vec{E}_j(\vec{r};\omega_1).\vec{E}_k(\vec{r};\omega_2).\vec{E}_l(\vec{r};\omega_3) \times \exp\left[-i(\omega_1+\omega_2+\omega_3)t\right]d\omega_1 d\omega_2 d\omega_3 \quad (10)$$

where $\chi^{(n)}$ is the n^{th}-order susceptibility defined as the Fourier transform of the response function of the material

$$\chi_{ijk}^{(2)}(-\omega_\sigma;\omega_1,\omega_2) = \int_{-\infty}^{+\infty} R_{ijk}^{(2)}(t_1,t_2)\exp\left[i(\omega_1 t_1 + \omega_2 t_2)\right]dt_1dt_2 \quad (11)$$

$$\chi_{ijkl}^{(3)}(-\omega_\sigma;\omega_1,\omega_2,\omega_3) = \int_{-\infty}^{+\infty} R_{ijkl}^{(3)}(t_1,t_2,t_3)\exp\left[i(\omega_1 t_1 + \omega_2 t_2 + \omega_3 t_3)\right]dt_1dt_2dt_3 \quad (12)$$

One can observe that the nonlinear response is a function of multiple wavelengths and the response is also time dependent. Laser wavelengths and pulse wave duration selected to conduct

measurements thus have a strong influence on the materials response since different nonlinear terms of the tensors can be involved.

For simplicity, at the macroscopic scale in the Fourier space, the polarization is usually seen as the sum of all the induced microscopic dipole moment. The material polarization is thus similarly described at the macroscopic scale by

$$P = \epsilon_0[\,\chi^{(1)}E + \chi^{(2)}EE + \chi^{(3)}EEE + \cdots\,] \tag{13}$$

where ϵ_0 is the vacuum permittivity, $\chi^{(1)}$ the linear susceptibility which is directly linked to the linear refractive index n_0, $\chi^{(2)}$and $\chi^{(3)}$ respectively the second and third order nonlinear susceptibilities and E the electric field. $\chi^{(2)}$ and $\chi^{(3)}$ nonlinear optical susceptibilities are tensors of the third and the fourth rank and contain 27 and 81 components, respectively. The susceptibilities exhibit various types of symmetry which are of fundamental importance in nonlinear optics: permutation symmetry, time-reversal symmetry and symmetry in space. The time-reversal and permutation symmetries are fundamental properties of the susceptibilities themselves, whereas the spatial symmetry of the susceptibility tensors reflects the structural properties of the nonlinear medium. The more general symmetry requirement that is currently used, called the overall permutation symmetry, is an approximation which applies when all of the optical fields involved in the susceptibility formulae (excitations and response) are far from any transition. This was first formulated by Kleiman [6] [7]

For centrosymmetric materials all components $\chi^{(2)}$ tensor are null. As a consequence, second-order nonlinear optical effects as well as first-order electro-optical effects are not observed in glasses and additional treatments of the material should be considered to break the centrosymmetry of glasses.

4. Nonlinear optical susceptibility

Second order, $\chi^{(2)}$, and third order, $\chi^{(3)}$, terms of the polarization have to be considered to describe nonlinear effects under intense optical excitations that may also be combined with strong static electric fields. These interactions are respectively called nonlinear-Optical (NLO) effects, that require only optical excitations, and Electro-Optical (EO) effects, where optical and electrical excitations are combined. A brief description of the basic EO and NLO effects and susceptibiities are gathered in Table 1.

Order	Tensor	Effect	Description
2	$\chi^{(2)}(-\omega ;\omega,0)$	Linear electro optical effect (Pokels's effect)	Under an electric field there is a change of refractive index in the NLO medium.
2	$\chi^{(2)}(0 ;\omega,-\omega)$	Optical rectification	A static electric field occurs in the NLO medium under illumination.
2	$\chi^{(2)}(-2\omega ;\omega,\omega)$	Second harmonic generation	The emission of light with double frequency happens under illumination of the NLO medium.
2	$\chi^{(2)}(-\omega_3 ;\omega_2,\omega_1)$	Generation of light with frequency equal to the sum of frequencies of incident radiations. $\omega_3 =(\omega_2+\omega_1)$	It is observed at illumination of the NLO medium by two light sources with different frequency. The frequency of emission equals the sum of the two excitation source frequencies.
3	$\chi^{(3)}(-\omega ;\omega,-0,0)$	Kerr's effect	Under the action of two electric fields there is a change of refractive index in the NLO medium.
3	$\chi^{(3)}(-\omega ;\omega,-\omega,\omega)$	Nonlinear refractive index also called Kerr's effect, self phase modulation.	The refractive index of the medium changes with intensity according to the formula: $n=n_0+n_2I$. Self-focusing and self-defocusing of a laser beam are special cases.
3	$\chi^{(3)}(-3\omega,\omega,\omega,\omega)$	Third harmonic generation.	There is an emission of light with triple frequency under illumination

			of the medium.
3	$\chi^{(3)}(-\omega_4;\omega_1,\omega_2,\omega_3)$	Multiwave mixing.	When illuminated with three light sources with different frequencies a generation of light occurs whose frequency equals the sum of the three excitation frequencies.

Table 1: Basic electro-optical and nonlinear-optical effects observed in dielectrics.

5. Third order nonlinearity in glass

In the absence of poling, or some other treatment to eliminate glass's isotropy, the first nonlinear term in vitreous material is $\chi^{(3)}$. In the relation (13) the electric field E appear three times in the third order NLO term introducing the possibility to combine three excitations at different frequency ω_i (with different field polarization). The $\chi^{(3)}$ susceptibility, which is described as shown in relation (12) the mixing of 4 electric field components (three excitation and 1 response), is a tensor of 3x3x3x3 with 81 terms (taking into account the combination of the electric field polarization). Indeed, the third order polarization can be written, without taking into account the degeneracy from the polarization state for clarity, in the frequency space as :

$$P(\omega_\sigma) = \varepsilon_0 \chi^{(3)}(-\omega_\sigma;\omega_1,\omega_2,\omega_3)\, E(\omega_1)E(\omega_2)E(\omega_3) \qquad (14)$$

The material can respond at a ω_σ frequency different from the excitation frequencies, while satisfying the two fundamental rules: that of energy preservation ($E = h\omega/2\pi$, where h is the Planck constant), and the preservation of momentum ($p=hk/2\pi$,) as described in figure 1 :

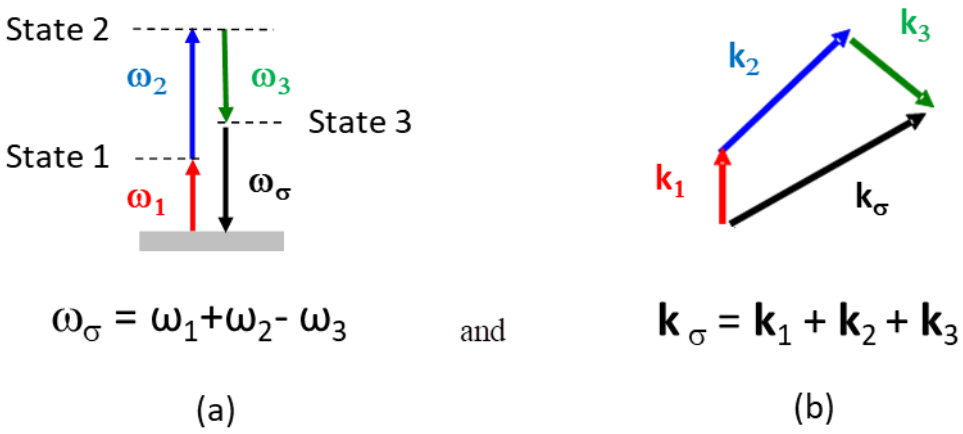

Figure 1: general case of four wave mixing : preservation of energy (a) and momentum (b)

Those figures express all the richness of high $\chi^{(3)}$ materials which allow four wave mixing phenomena.

Transparent media (out of resonance): When considering transparent materials (out of any resonance), none of the intermediate states 1, 2 or 3 in our example is corresponding to an electronic or vibrational state of the materials. Two responses can be identified: the Kerr effect and the third harmonic generation (THG).

- Kerr effect: in the degenerate case for which the NLO response is observed at the same frequency as that of the excited beam, the term $\chi^{(3)}(-\omega; \omega,-\omega,\omega)$ can be considered. This term gives rise to the nonlinear Kerr effect in glass and results in the refractive index variation, $n = n_0 + n_2 I$, with I being the light intensity, n_0 the linear refractive index and n_2 is called the nonlinear refractive index. The Kerr effect is responsible for the self-focusing phenomenon and the self-phase modulation which leads to the spectral broadening of the pulse. Such an effect can be used for soliton wave propagation or fast optical switches.

- THG : For intense excitation with a monochromatic wave, the generation of a triple frequency signal can be observed thanks to the term $\chi^{(3)}(-3\omega;\omega,\omega,\omega)$. Such response can be

used for imaging in space the third order nonlinearity by coupling the measurement with an optical microscope for instance. [3]

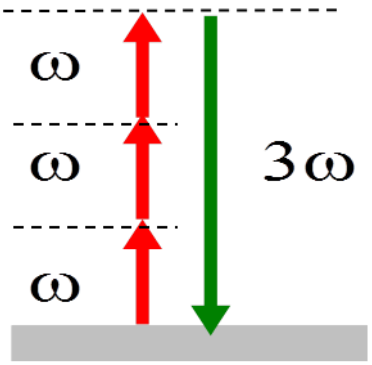

Figure 2: Schematic energetic diagram of the THG phenomenon

Absorbing medium (resonance) : At least one intermediate state 1, 2 or 3, in the example, corresponds to a real electronic or vibrational state of the material. For instance, in the case of the two photon absorption or the stimulated Raman effect, the imaginary term of the $\chi^{(3)}$ susceptibility is involved.

- Two photon absorption : In a transparent spectral region, far from a possible linear absorption, two photons can be simultaneously absorbed if the density of photon is sufficient. In most case, such criterion is only fulfilled in the focalization volume. The nonlinear absorption is commonly used for 3D control of the laser induced modification.

➢

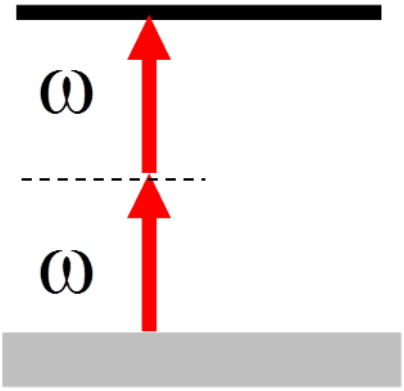

Figure 3: Energetic diagram of the two photon absorption

➢ Stimulated Raman : Raman amplification, or Raman gain, is a nonlinear optical process that is based on the stimulated emission of a photon at a frequency that is down-shifted by the vibrational modes of a medium. Two laser beams, presenting a frequency difference matching a vibrational state of the material, interact in the volume of the medium and light intensity can be transferred from the first beam (ω_1) to the second beam (ω_2). The difference (ω_1-ω_2) of the pump beam and the beam to amplify (signal) corresponds to the frequency Ω from the fundamental state to the excited vibrational state.

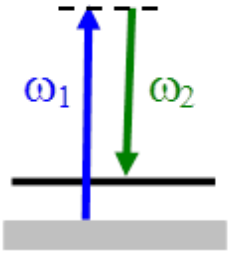

Figure 4: Energetic diagram of stimulated Raman effect involving a vibrational excited state

5.1 Kerr effect in glass

5.1.1 Physical phenomena contributing to the nonlinear index

Historically, the optical Kerr effect is the nonlinear optical property that has been the most studied in glass. Four main phenomena are contributing to the nonlinear refractive index with a different origins and with different time responses: thermal, electrostrictive, nuclear and electronic :

$$n_2 = n_2^{electronic} + n_2^{nuclear} + n_2^{electrostrictive} + n_2^{thermal} \qquad (15)$$

The electronic and nuclear responses originate from the oscillation of the electronic cloud combined, or not, respectively with the vibration of the nucleus. While the electronic response is related to the spontaneous nonlinear distortion of the electronic distribution around the nuclei, the nuclear response is due to a slower optical-field-induced change arising from the motions of the nuclei. The nuclear associated response has led to limited investigation. It has been usually considered to contribute 10 to 15% of the total n_2, but such assumption has to be taken with precaution depending on the glass composition and the laser characteristics.[8]

Far from a resonance, the pure electronic cloud contribution is the fastest with characteristic time less than one femtosecond. For isotropic materials, the third-order susceptibility tensor far from resonance can be fully defined by the measurement of only one term of the $\chi^{(3)}$ tensor thanks to the following relation. [7]

$$\chi^{(3)}_{xxxx} = 3\chi^{(3)}_{xxyy} = 3\chi^{(3)}_{xyxy} = 3\chi^{(3)}_{xyyx} \qquad (16)$$

The nuclear contribution to $\chi^{(3)}$ originates from the rearrangement of the position of the nuclei during the excitation. This effect is much slower than the electronic one, it is on the order

of several hundreds of femtoseconds to a few picoseconds. Because of this timescale, the impact of the nuclear contrubution will then be highly correlated to the laser pulse duration.

The electrostrictive contribution corresponds to the material density variation when submitted to an electric field. This effect has a response time of the order of tens of nanoseconds similar to that of an acoustic wave in the material. The thermal response is due to the absorption of the electric field by the material and its dissipation by heat. The response time of thermal effects is on the order of tens of microseconds.

When fast response time is considered below few hundred picosecond regime, within the Born-Oppenheimer approximation, only the electronic and the nuclear contributions contribute to the Kerr effect.

5.1.2 Third order nonlinearity scale in glass

The nonlinear refractive index evolution tendency versus the different glass family (selenide, sulfide, oxide, fluoride) is now established, thanks to almost 30 years of continuous investigations. (figure. 5). Due to the four wave mixing based phenomenon, special attention is necessary while selecting the laser wavelengths for measuring the non-resonant nonlinear response. For instance, when evaluating the third order nonlinearity by THG, it is necessary not only to select a fundamental wavelength ω far from any absorption but also to pay attention to the third harmonic wave 3ω which should be also out of resonance. This requires, for materials with a band gap in the visible range, to select a laser wavelength ω as high as possible in the near infrared.

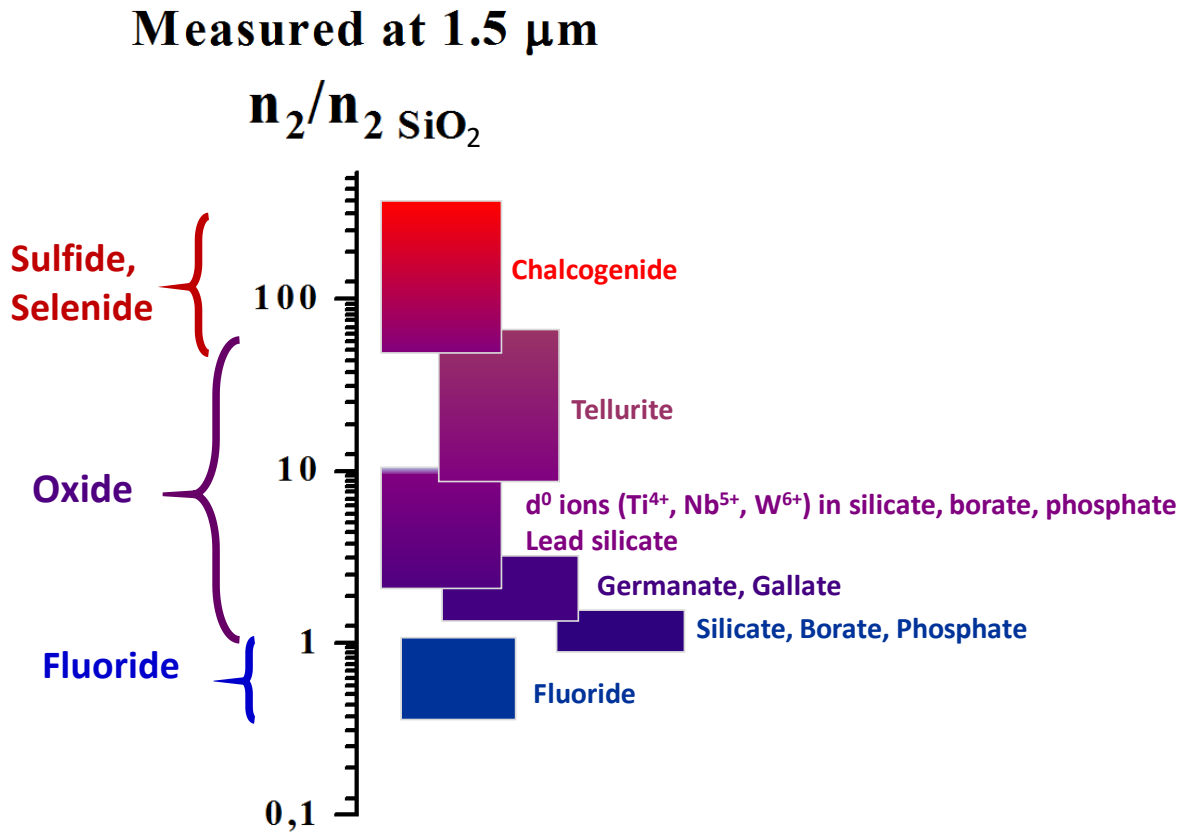

Figure 5: Scale of third order nonlinearity (Kerr effect) among various glass compositions. (The color coding from blue to red is a qualitative indication of the magnitude of nonlinear materials response for the eye)

It has been established that the fast response time Kerr effect (1 picosecond) out of resonance is, in a first approximation, following the evolution the glass polarizability and more precisely the polarizability of the anions ($F^-<O^{2-}<S^{2-}<Se^{2-}$) (Figure 5). Several studies have also established a correlation between the decrease of the material band gap and the increase of the nonlinear optical behavior. For instance, SiO_2 has a band gap about 9 eV, niobium phosphate around 3.5 eV and As_2S_3 around 2.3 eV. One notices that this progression goes along with a strong reduction of the damage threshold for measurement in the NIR. Several models have been proposed to estimate the nonlinear response of glasses. The model proposed by Sheik Bahae et al. for crystalline materials has been applied, for instance, to estimate the values of n_2

using a simple Kramers-Kronig analysis by the approximation of the two-photon-absorption spectrum by a two-parabolic-band model (semiconductor model approximation).[9] This model allows determination of the order of magnitude of the glass response even if as mentioned by Harbold et al., precaution needs to be considered since this model does not take into account the exponential Urbach tail of the amorphous materials. [10]

When considering a specific glass family, it appears that the evolution is complex and the impact of the glass structure and composition has a huge impact on the nonlinear optical responses of the material. Different investigations have been conducted by different research groups in order to establish structure property relationship.

Regarding oxides, silicates, phosphates and borates, the introduction of alkali and alkaline earth ions by forming non-bridging oxygen between the glass formers increases the linear and the nonlinear indices. Nasu et al. in 1995 clearly established that in silicates, the introduction of alkali or alkaline earth ions increases the nonlinear optical response thanks to the formation of non-bridging oxygens having higher hyperpolarizability than bridging oxygens.[11]

The introduction of d^0 transition ions (with empty d orbitals) in silicate, phosphate and borate glass matrices allows a drastic increase in the nonlinear optical response without resonance phenomenon. [4] [12] It has been demonstrated that the arrangement of the structural units formed mainly of MO_6 octahedra, with M the transition metal ions, has an important impact on the nonlinear response of the glass. In the specific case of niobium and titanium, the formation of a 2D or 3D network of MO_6 octahedra for high concentration of transition metal oxide leads to a strong increase of the n_2 (≈10 times that of SiO_2). For the titanium oxide, chains of distorted TiO_6 have been evidenced, while for niobium oxide the network organizes as a tridimensional corner shared NbO_6 skeleton. Such high nonlinear index can be also obtained by incorporating high concentration of ions with a lone pair of electrons ns^2 such as Pb^{2+} in silicate based glass composition.

Nonlinear optical properties more than 10 times silica can be obtained in lone pairs of electron ns^2 oxide based compounds. It is the case for instance of tellurite glass composition in which the tellurium oxide amount can reach 99% of TeO_2 [13]. The Te^{4+} ion occupies a TeO_4 disphenoid site where the tellurium ion is at the center of a trigonal bipyramid TeO_4E in which the electronic doublet E form the third equatorial corner. When the concentration of TeO_2 decreases by adding modifiers such as Al_2O_3 for instance, the TeO_4 entities are progressively replaced first by asymmetric groups TeO_{3+1} corresponding to TeO_4 disphenoids with a Te-O axial long bond and by trigonal pyramids TeO_3 for the largest modifier concentration. The origin of the nonlinear optical properties has been related to the strong optical hyperpolarizability of the TeO_4 entities forming a chain-like structure [14] [15] The effect of a glass modifier on the chain-like structure will then have a strong influence on the nonlinear optical response of the materials. Modifiers such as ZnO tend to rapidly break the tellurite chains and to decrease the magnitude of the nonlinear response. The highest nonlinear indices observed in tellurite glass have been obtained when the TeO_2 is combined with other ions also having a ns^2 lone pair of electrons such as Tl^+, Pb^{2+} or Bi^{3+}.[16] [17] Table 2 reports the nonlinear third order susceptibilities measured at 1.5 µm on various tellurite glass compositions. Depending on the glass modifier, different values can be observed with the following evolution $d^{10} < ns^2np^6 < d^0 < ns^2$.

Glass composition (Mol%)	Third order susceptibility $\chi^{(3)}$ (10^{-23} SI) ± 20%
$90TeO_2$-$10Tl_2O$	141
$90TeO_2$-$10Nb_2O_5$	115
$90TeO_2$-$10WO_3$	97
$90TeO_2$-$10Al_2O_3$	78
$90TeO_2$-$10Ga_2O_3$	72
$90TeO_2$-$10Sb_2O_4$	58
SF59 (lead silicate)	57

Table 2 : Nonlinear susceptibility of different tellurite glass measured at 1.5µm

As explained by Jeansannetas et al. [18], the largest nonlinear response is generated by heavy cations having ns^2 electron pairs such as Bi^{3+}, Pb^{2+} or also Tl^{+} ions. The addition of Tl_2O in the tellurite glass matrix leads to high magnitude of optical nonlinearity [18] [16] but is at the expense of depolymerization of the glass network and a reduction to the glass' stability [19] [20]

Chalcogenide glass (sulfide, selenide) present the largest nonlinear index with n_2 above 80 to more than 500 times the SiO_2 value for measurement in the near infrared range. As_2S_3 glass has a n_2 at 1.5µm for instance 80 times higher than the SiO_2 value. In such materials, the materials composition and structure has also an impact on the nonlinear optical properties. First of all, the substitution of sulfur by selenium leads to a continuous increase of the nonlinear optical properties for measurement at 1.5 µm. A strong increase can be observed when Se/S ratio is above 1 with n_2 4 times higher in As_2Se_3 glass than in As_2S_3.[21] [10] Such increase has to be related to a decrease of the bandgap of the materials which should lead to a dispersion of the nonlinear optical response and the appearance of a two photon absorption resonance. In such materials when the concentration of (S+Se)/As is above 1.5, an increase of the nonlinear optical properties have been noticed in various study for rich selenium content materials even if the evolution of the band gap structure is not significant. This effect has been related to the formation of highly hyperpolarizable Se-Se bonds.[21] A similar increase of the nonlinear optical properties for substitution of sulfur for selenium has been measured in the glass system Ge-Sb-S-Se. Germanium selenide glass has a n_2 at 1064 nm ~350 times the n_2 of SiO_2. Correlations have been established by X ray photoelectron (XPS) between the nonlinear optical response and the presence of Ge-Se and Sb-Se bonds. The nonlinear response within the glass system Ge-Sb-S can be increased by substituting germanium for gallium.[22] Even if the nonlinear response of the chalcogenide is large, when considering applications, the issue

remains the ratio between the nonlinear response and the absorption. Early in 1989, a figure of merit was proposed, being FOM = $n_2/\beta\lambda$ with β the nonlinear absorption coefficient and λ the wavelength.[23] It has been proposed that selenium containing glasses in the system As-S-Se or Ge-Se-Sb could offer large Kerr effect with n_2/n_{2SiO2} respectively of 500 and 360 while satisfying an optimized FOM for use in the near infrared range.[24] [10]

5.1.3 Influence of the nuclear contribution in glass

n 1975, Hellwarth *et al.* have showed that the nuclear contribution to the nonlinear refractive index of some glasses is not negligible and can reach as high as up to 15–30 % of the total nonlinear response depending on the glass composition [25] Later Smolorz *et al.* have, for instance, demonstrated that the relative nuclear contribution to the nonlinear refractive index increases upon addition of GeO_2 in a SiO_2 optical fiber from 13% to 18% for respectively molar percentage of GeO_2 in SiO_2 ranging from 0 % to 16% in molar percentage.[26] In 1992, Stolen et al. pointed out that such nuclear contribution is highly dependent on the pulse width and decreases below ~100 femtoseconds.[27] Several groups have actually experimentally shown that the nuclear contribution is definitely dependent on the laser pulse duration and especially for ultrafast laser regime. [27] [28] The time dependent observation of the nuclear motion has to be fully taken into account in equation (7). This Raman contribution to the nonlinear refractive index constitutes a non-instantaneous nonlinear response in a femtosecond regime. The effect is clearly seen when the optical pulse width becomes comparable to the molecular resonance period. Based upon the Born-Oppenheimer approximation, several measurements of the nuclear contribution in glasses have been performed in the femtosecond regime using time-resolved techniques to separate out the electronic and the vibrational contributions. [8] [29] [30] The nuclear contribution can be obtained by integrating the overall Raman cross-section while taking into account the depolarization ratio as proposed by [31]:

$$n_2^{nuclear} = \frac{2\pi c^4}{n_0 \hbar \upsilon_P} \int_0^{\infty} \frac{\left[1 - e^{\frac{-\hbar\omega}{kT}}\right]}{\upsilon_S^3 \omega} \frac{\partial^2 \sigma_{//}(\upsilon_P, \omega)}{\partial\Omega \partial\omega} d\omega \qquad (17)$$

Where υ_P is the pump frequency, υ_S is the signal frequency, ω is the Raman frequency (Stokes shift), Ω is the frequency shift, and $\frac{\partial^2 \sigma_{//}(\upsilon_P, \omega)}{\partial\Omega \partial\omega}$ is the parallel polarization component of the spontaneous Raman cross-section. Heavy metal oxide and chalcogenide glasses have been investigated since they offer the largest nonlinear response. For instance, S. Smolorz et al. reported for 57.2 PbO-24.9 Bi_2O_3-17.8 Ga_2O_3 and 7.5 BaS-17.5 Ga_2S_3-70 GeS_2 respectively 9% and 18% of the nuclear contribution to the total n_2. [26]

Among the different glass families, glasses containing transition ions with empty d orbital and especially niobium oxide have been widely studied. They can exhibit high nonlinearity in various glass matrices for incorporation of a large amount of Nb_2O_5.[32] [33] The increase of the third-order nonlinear optical response has been directly related to the atomic density of transition ions in the glass. In addition, a particular behavior of the nonlinear refractive index has been shown, with a clear enhancement of the nonlinear optical response for large amount of niobium ions in the glass network (Figure 6).

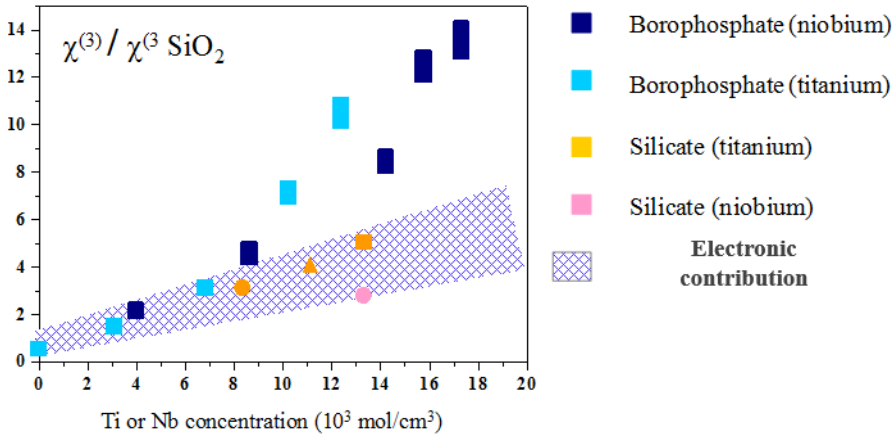

Figure 6: Evolution of the relative third order nonlinearity to SiO_2 of d^0 transition ion containing glass versus titanium or niobium volume concentration

In the specific case of the introduction of niobium oxide in phosphate or borophosphate glass matrices, the optical nonlinear response has been related to the specific three-dimensional corner-sharing arrangements of NbO_6 octahedra, which enables the formation of a tungsten bronze-like local structure for high niobium oxide concentration. Lipovskii *et al*. have observed similar behavior of the electro-optical Kerr effect, with the successive addition of Nb_2O_5 into silicate-based glasses.[32] All those investigations have illustrated the correlation between the increase of both the Raman spectral density and the Kerr response of the materials with an increase of NbO_6 tungsten bronze "crystal motifs" within the glass structure. The enhancement of the nonlinear response in niobium oxide containing glass belongs to the nuclear contribution to the nonlinear response, which can reach 40% of the overall Kerr effect for high niobium oxide concentration (Figure 6). The nuclear contribution, as mentioned before, is definitely dependent on the laser pulse width. As shown in figure 7A and 7B for respectively silica and niobium oxide phosphate glass, the nuclear contribution rapidly drop when pulse width are below 100 fs to become negligible for laser pulse width below 10 fs. On the contrary the phenomenon is clearly at its maximum for picosecond laser regime.

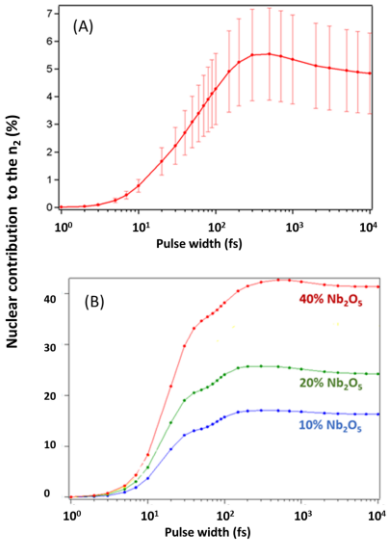

Figure 7 (A) Nuclear contribution to the nonlinear response for SiO_2 versus the laser pulse width, (B) nuclear contribution to the nonlinear response for a $NaPO_3$ glass matrix with various amount of niobium oxide. (for clarity, the error bars of 20% on the nuclear contribution have not been displayed on the graph (A))

The niobium oxide containing glasses illustrate the importance of taking into account the laser regime when evaluating the nonlinear response of the glass. It also illustrate the variety of the magnitude of the nuclear contribution to the nonlinear index among different glass compositions.

5.2 Raman gain

C.V. Raman first discovered the spontaneous Raman scattering process in 1928, for which he received the Nobel Prize in 1930. [34] More than three decades later, stimulated Raman scattering was discovered by Woodbury and Ng in 1962, but it was not until 1973 that the first experimental evidence of stimulated Raman process, or Raman amplification, in an optical fiber was actually observed by Stolen and Ippen. [35] Raman amplification is a nonlinear optical process that is based on the stimulated emission of a photon at a frequency that is down-shifted

by the vibrational modes of a medium. From a classical mechanics point of view, the Raman gain process is described by the imaginary part of a nonlinear susceptibility $\chi^{(3)}$, in which a signal beam gets amplified by a pump beam, given that the difference in energy between the two beams goes into the vibrational modes of the Raman gain medium.

The gain magnitude depends on the pump wavelength and on the material properties (e.g. frequency of the Stokes shift, and Raman spectral intensity), as shown with the example of SiO_2 in Figure 8. The selection of various pumps at different wavelength permits amplification within the transparency windows of glasses.

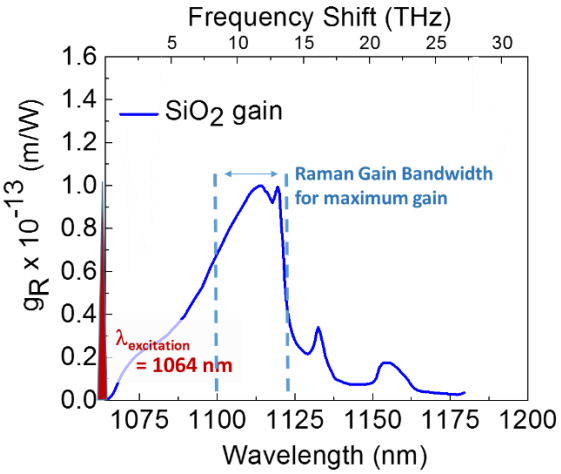

Figure 8: Raman gain spectra of silica glass, with a pump laser at 1064 nm. Here the gain bandwidth is defined by the full width at half maximum (FWHM).

Even in the early days of fiber optics [36], the fundamental advantages of Raman amplifiers were evident even if, for telecommunication, erbium-doped fiber amplifiers (EDFA) have been rapidly adopted thanks to the requirement of much lower pump power for operation [37]. Traditionally, there are several types of Raman amplifiers, one of which is the distributed Raman amplifier. In this case, the gain is accomplished along the propagation length throughout the optical fiber itself; hence, the trade-off between the gain and the optical losses becomes an

essential factor to achieve high performance. This category can further be expanded into cascaded or diode pumped distributed Raman amplifiers, respectively. Such Raman amplifiers are primarily used in the long-haul network systems. These types of amplifiers require a gain medium with high gain coefficients and broad bandwidth; and in this case, low loss is a desirable property but not a crucial issue. Another type of application is Raman fiber lasers, in which the device operates as a typical laser system [38].

Several glass families were studied during the 1970s and 1980s with the purpose of increasing the scattering cross-section [39], [40], [41], [42]. Among the main oxide glass systems studied were silica, germanium-doped silica glasses, and multi-component glasses such as heavy metal oxide glasses.

Fused silica has been the key material used for long haul transmission of optical signals, thanks to its good optical properties and low loss characteristics, which give attractive figure of merit (described as the trade-off between Raman gain and losses). Indeed, the most studied Raman gain media have been fused silica and germanium-doped silica glasses [43], [44], [45], [46]. However, fused silica offers a limited usable bandwidth for Raman amplification of 5 THz and has one of the lowest Raman cross section among glasses (Raman gain magnitude of g_R=0.89x10^{-13} m/W at 1 μm). Another glass matrix that has been investigated as a Raman fiber amplifier is phosphosilicate, which provides peak Raman gain of 40 dB at 1.3 μm. [47], [48]

Heavy metal oxide glasses have been proposed for Raman gain applications due to their enhanced nonlinearity and transparency over the telecom window for fabricating short components. [42] [49] Tellurite fiber has been also evaluated for its high Raman gain performance (gain over 10 dB) with relative low loss of 20 dB/km [50]. Glass families which primarily include TeO_2-based glasses for high gain applications have been recently reported in the literature, [51] [52] [53] [54] [55].

In 2005, Stegeman et al. demonstrated that direct Raman spontaneous cross section measurement can be used for estimating the Raman gain coefficient after careful correction using the Bose-Einstein factor [35], [54]. Using such an approach, it has been demonstrated that the introduction of transition ions in phosphate or borophosphate glass matrices allows reaching a Raman gain coefficient close to 10 times the value of silica (Figure 9).

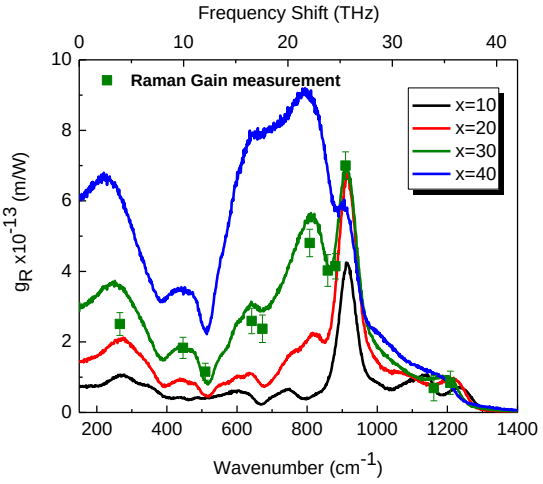

Figure 9 **:** Calculated Raman gain curve, from spontaneous Raman cross-section measurements of phosphate (100-x) $NaPO_3$ – x Nb_2O_5 glass system (extracted from VV polarized spontaneous Raman spectra), normalized to SiO_2, along with experimentally-measured Raman gain coefficient data points of composition 70% $NaPO_3$ – 30% Nb_2O_5, using direct NLO technique at 1064 nm

A broad-band amplification window has also been shown by introducing small amounts of d^0 ions in the phosphate, thanks to the disruption of the phosphate chains and the formation multiple phosphate units with various vibration signatures such as in figure 10 leading to a Raman gain bandwidth of 38 THz as compared to the 5 THz of fused silica. [56]

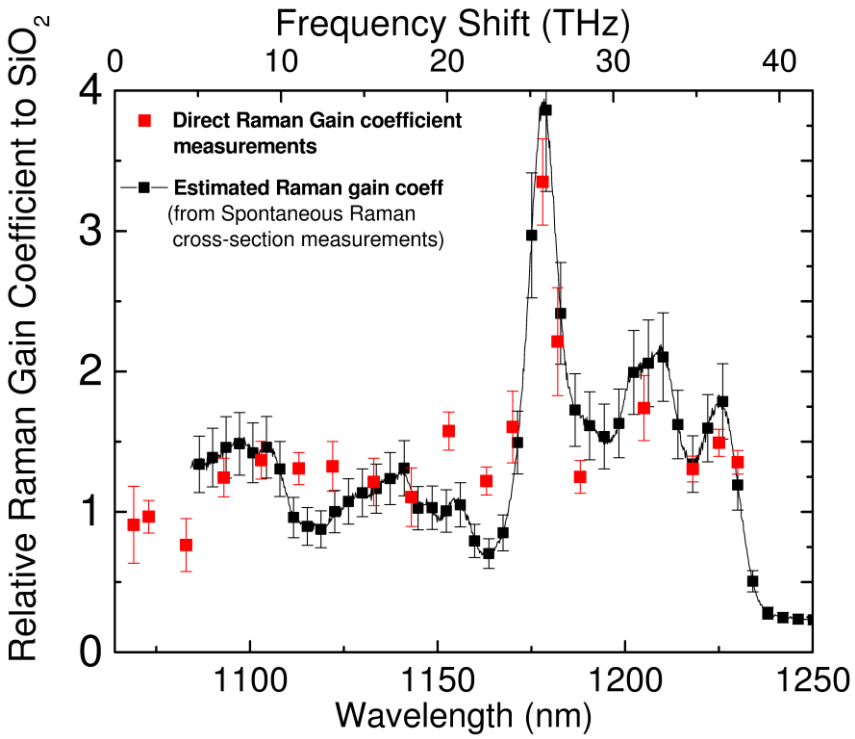

Figure 10 : Calculated (black) and experimental (red) Raman gain spectra of glasses 90% $NaPO_3$ – 5% $Na_2B_4O_7$ – 5% TiO_2

Heavy metal oxides can provide a high Raman cross section. Among such materials, tellurites have been widely investigated. Using classical melting methods, pure TeO_2 glass cannot be obtained, requiring minor (a few mol%) additions of modifiers to avoid crystallization. Previous investigations have shown that the introduction of d^0-transition ions (W^{6+}, Nb^{5+}, Ta^{5+},Ti^{4+},etc.) or ions with a lone pair of electrons such as Tl^+ or Pb^{2+} to the TeO_2 glass network former, allows one to maintain high optical nonlinearity, high Raman gain and to improve the processing conditions required to make high quality glass [54], [57], [58].

Several glass compositions have been investigated, and Table 3 reports binary glass compositions for the introduction of different intermediate compounds. The main contributions to the Raman spectrum correspond to the vibration at around 665 cm^{-1} and 750 cm^{-1};

respectively assigned to the presence of TeO_4 bi-pyramids, and to the TeO_{3+1} or TeO_3 trigonal pyramids vibrational units. In the case of d^0 transition ions, the most intense contribution is the 665 cm^{-1} vibration. It has been recently demonstrated that in such glass the existence of the Te-O-Te chains formed with TeO_4 units is the source of the nonlinear optical response. Introduction of zinc oxide into the composition, resulting in the disruption of those chains, induces a fast drop of the nonlinear optical response.[59]

For tellurite glass compositions with lone pairs of electron, such as thallium, the TeO_3 vibration can become the most intense and lead to Raman gain coefficient 50 times the value of fused silica at 1064 nm as reported in table 2 and Figure 11.

Glass Composition		**TeO_4 (υ=665 cm^{-1})** g_R **x 10^{-13} (m/W) ± 20%**	**TeO_3 (υ=750 cm^{-1})** g_R **x 10^{-13} (m/W) ± 20%**
85%TeO_2 – 15%WO_3		43	25
85%TeO_2 – 15%TiO_2		39	16
85%TeO_2 – 15%$NbO_{2.5}$		44	17
85%TeO_2 – 15%PbO		36	31
85%TeO_2 – 15%$GaO_{1.5}$		26	13
x TeO_2 – (100-x) $TlO_{0.5}$	x=75%	25	19
	x=70%	21	23
	x=50%	14	52±3

Table 3. Composition of different binary TeO_2 glasses, Raman Gain measurement at 1064 nm

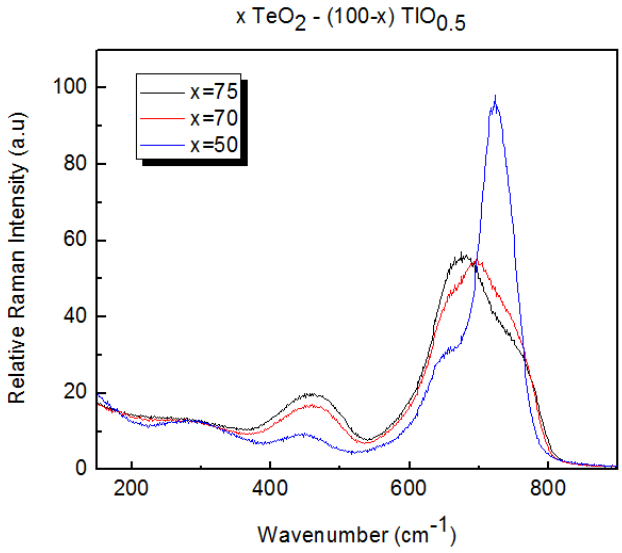

Figure 11 : parallel/parallel polarized (VV) spontaneous Raman spectra of the x TeO_2 – (100-x) $TlO_{0.5}$ glass system, normalized to SiO_2. Excitation wavelength 514 nm

Special attention should be paid while measuring or estimating the Raman gain coefficient. As demonstrated by Rivero et al., large decrease in the relative intensity of the Raman scattered signal with increasing excitation wavelength between 458 and 752 nm is clear (Figure 12). [60] Since all the spectra have been normalized to SiO_2, this result clearly illustrates a strong dispersion dependence of the Raman susceptibility tensor. This effect has to be taken into account while comparing Raman gain measurements in the literature measured at different wavelengths.

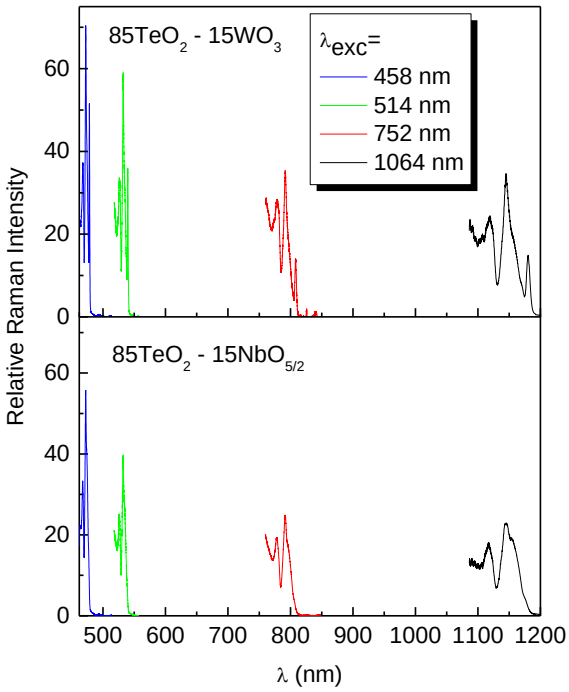

Figure 12 : VV polarized experimentally-obtained spontaneous Raman Spectrum for $85\%TeO_2 – 15\%NbO_{2.5}$ and $85\%TeO_2 – 15\%WO_3$ tellurite glass composition normalized to SiO_2 traducing the dispersion of the Raman response for different excitation wavelength.

Chalcogenide glasses offer the largest Raman Gain coefficient in the near infrared. Chalcogenide fibers (As_2S_3 and As-Se fibers), can provide Raman gain coefficients several hundred times that of SiO_2. [61], [62] Such an effect is directly linked to the high nonlinear third order susceptibility of such compositions but also to the dispersion phenomenon. Tohoutek at al. have reported high Raman gain for sulfide in the glass system Ge-Ga-Sb-S. [63] Within the vibration mode domain between 250-500cm^{-1}, for measurement at 1064 nm by comparing the measured Raman scattering intensities with the Raman intensity of the silica glass, peak gain of 296 and 140 have been measured respectively for As_2S_3 and GeS_2. Nevertheless, one has to keep in mind that the use of such glasses requires the selection of pump wavelengths at $\lambda>2\mu m$

in order to avoid detrimental nonlinear absorption phenomena. For selenides, at 1550nm, using As_2Se_3 fiber, Slusher et al. reported a Raman gain of 780 times the value of SiO_2. However, as reported by various authors the issue of the material stability for use in the near infrared should be taken into account.[64]

5.3 The specific case of Supercontinuum Generation

Supercontinuum generation in glass fiber, which is a wide spectral broadening of a intense laser beam thanks to an addition of multiple nonlinear processes has become, during the last decades, a hot topic. The nonlinear optical phenomena at the origin of the spectral broadening can be multiple, depending on the material and the adopted optical and materials configuration. Alfano et al. first reported the supercontinuum generation in glass. [65], [66] In the end year of 1990's, the discovery of the "photonic crystal fiber" which allows taking advantage of nonlinear optical properties and managing the group velocity dispersion and the position of the zero wavelength dispersion have led to the demonstration of broad spectral generation out of fiber systems. [67] Supercontinuum generation has found numerous applications such as spectroscopy, pulse compression, and in the use of tunable ultrafast femtosecond laser sources. The physics of spectral broadening is complex. When seeded by femtosecond pulses for instance, in the early stage, self-phase modulation takes place and later, various phenomena occurs such as stimulated Raman scattering, four wave mixing etc. [68] Even if the silica remains the best materials for visible range, when the near infrared or mid infrared range is required, novel materials with low phonon energy need to be developed. Again, the loss issue is crucial but also the transmission window of the glass. Silica-based photonic crystal fiber offers supercontinuum generation with flat spectral power densities, however, SiO_2 is not transparent above 2400nm. Recently Jiang et al. demonstrated that fluorides allow extended use in the infrared but also in the ultraviolet range, spanning more than three octaves in the spectral range 200–2500 nm.[69] Heavy metal oxide glass or chalcogenide glasses are interesting alternative for transmission in the MidIR

since they have high nonlinear optical response for shortening the final device and they allow expending the transmission spectrum in the infrared thanks to their low phonon energy. Much effort has been deployed to improve the glass optical quality and to engineer group velocity dispersion management using suspended core technology as shown in Figure 13

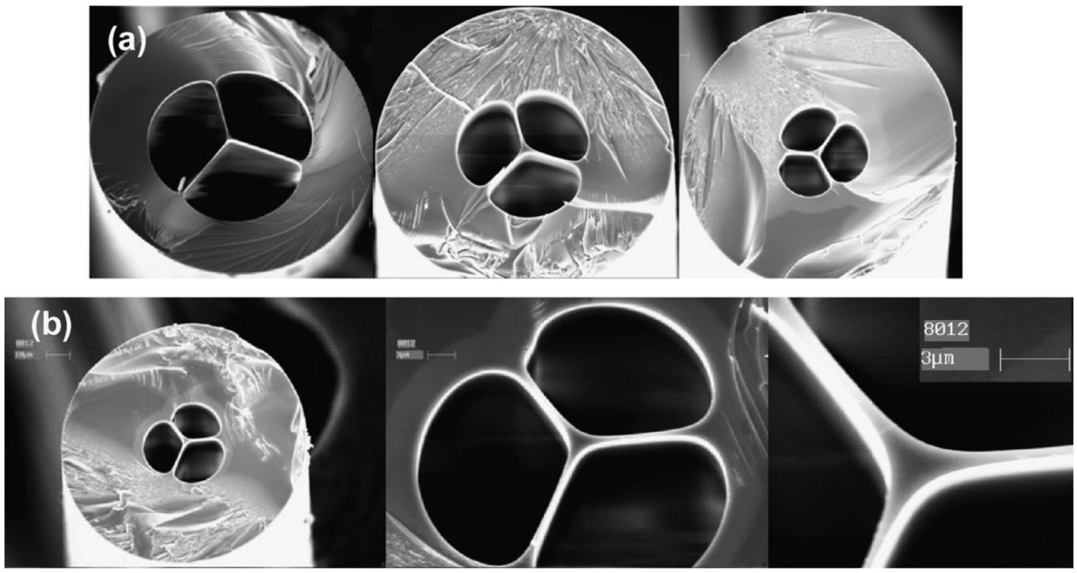

Figure 13 : SEM images of various tellurite glass micro structured fibers (a) core diameters varying from 1.6 to 2.2 µm. (b) the same fiber at different scales .[70]

In the case of tellurite glasses, large spectral broadening has been demonstrated with bandwidth exceeding 2500 nm while managing the zero dispersion by micro structured fiber in tellurite suspended core fiber thanks mainly to OH absorption band reduction.[71], [72], [73] [74] [75] In chalcogenide glasses, using suspended core $As_{38}Se_{62}$ fiber, Moller et al., using a laser source exciting in the MidIR, emiting at 4.4µm, demonstrated in 2015 a supercontinuum spanning from 1.7 to 7.5 µm with an average output power of 15.6 mW. [76] Suspended core fiber can present drawbacks since surface contamination can become an important issue with formation, for instance in chalcogenides, of oxide impurities which dramatically reduce the transmission window of the fiber. [74] Recently, major efforts have been conducted to engineer step index

fibers which prevent air contact with the core using newly available MidIR lasers close to the minimum dispersion wavelength of the core materials. [77] Using such an approach, mid-infrared supercontinuum covering the 1.4–13.3 μm spectral range has been demonstrated using chalcogenide step-index fiber formed of a $As_{40}Se_{60}$ core surrounded by a $Ge_{10}As_{23.4}Se_{66.6}$ cladding pumped at 6.3μm (Figure 14). [78]

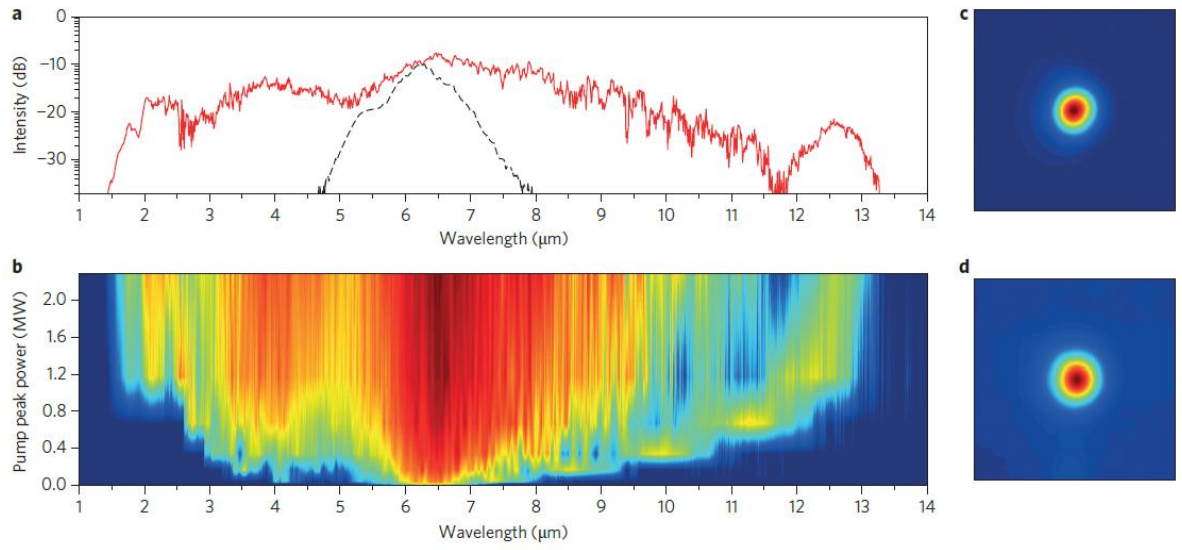

Figure 14 : Experimental Supercontinuum generation with the pump laser centred at 6.3 μm. a, Input pump spectrum (dashed line) and spectral profile at maximum pump power (solid line b, Spectral evolution with increasing pump peak power, showing the gradual redshift of a distinct spectral peak at the long-wavelength edge and the corresponding formation and blueshift of dispersive waves. c,d, Fiber output near-field beam profile corresponding to the spectrum in a for all wavelengths (c) and beam profile for wavelengths above 7.3 μm only (d) [78]

6. Second order optical properties in glasses

Second order non-linear (SONL) optical responses are of an utmost importance in photonic application. The most common uses are notably for electro-optical signal conversions and optical frequency control. At a first level of description, if one considers a centrosymmetric material and only the electric-dipolar optical response, it implies that the even nonlinear dielectric susceptibility, $\chi^{(2)}$, is zero. Under this approximation, symmetry requirements do not allow nonlinear optical response of the second order in any homogeneous glassy material. However, several second harmonic optical signals, having different origins, can be observed in glasses. First, the second harmonic elastic scattering or Hyper Rayleigh, which can be measured in all kind of inorganic glass. This harmonic diffusion signal can be linked to the second order molecular hyperpolarizability, β (Equ. (2)). This signal is commonly used as a spectroscopic tool to study isotropic media such as liquids or glasses. [79] [80] Second, at the glass surface, a structural loss of the inversion symmetry at the interface allows the observation of a coherent second harmonic generation having an electric-dipolar origin. Third, even in the bulk, second order optical response have been measured and linked to electric-quadrupole and magnetic-dipole contributions. [81] [82] [83] Please note, that such origin of the optical nonlinearity were not described in the previous sections which was only focused on electric-dipole contribution. The understanding of these optical signals is of a great importance for the development of second harmonic generation as a tool for interface characterizations, or structural studies. Nevertheless, the efficiency of second order optical responses observed in homogeneous glasses remains very weak and can be hardly considered for photonic applications.

To implement effective $\chi^{(2)}$ in glasses, poling treatments have been widely used to break the centro-symmetric nature of a glass structure. Poling can be based on the action of a laser irradiation, called optical poling; [84], on the action of an external electric field, called thermal (electrical) poling or corona poling; [85] ,[86] and also on the action of electron beam

irradiation [87] or proton implementation. [88] Within all these different kind of poling methods, optical and thermal electric poling are the most studied approach in the literature to induce efficient second order optical properties in glasses and will be reviewed in the next sections.

6.1 Second order optical response by optical poling.

In 1981 Sasaki et.al were the first to report the observation of a second order optical response in an inorganic oxide glass. A peak pump power of 0.8kW at 1064nm from a Q-switched and mode-locked Nd:YAG laser were injected in germanosilicate fibers. As shown in Figure 15, the authors demonstrated two wave sum-frequency responses between the laser pump (ω_p) and the two first Raman stokes signal (ω_1 and ω_2) resulting in the signals ωs_1 and ωs_2 [84].

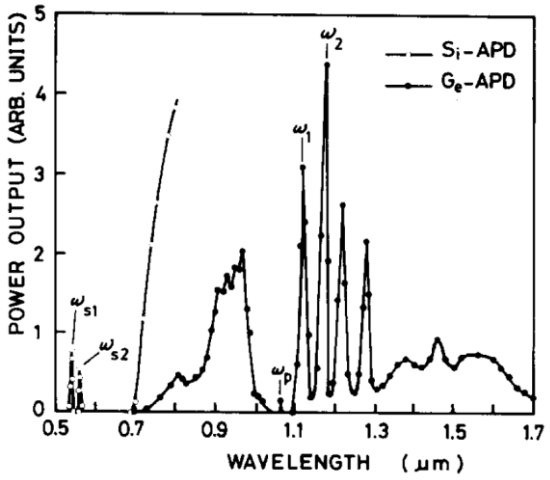

Figure 15 : Two wave sum-frequency response spectrum measured by Sasaki et al. for injection in a germanosilicate fiber of a signal at 1064nm from a Q-switched mode-locked Nd:YAG laser. The measurements were done using two detectors a silicon and a germanium avalanche photodiode (Si-APD and Ge-APD as noted in the figure legend) [84].

Five years later, an efficient second harmonic generation response were observed in single mode germano silicate optical fiber illuminated by a Nd:YAG laser producing up to 70kw peak

power of 100-130-psec- pulses with a 1250 Hz Q-switched rate. Within the first 9 hours of the illumination procedure, the SHG efficiency grew exponentially over more than 4 orders of magnitude and finally saturate after approximately 12 h. Österberg et al. observed in this experiment a peak power-conversion efficiency of 3%.[89]

Stolen et al. have demonstrated the importance of a co-illumination with a strong power at the fundamental frequency with a second weak "seeding" illumination at the harmonic wavelength, in order to greatly increase the speed of the second order optical response implementation in the fiber. Moreover, these authors have demonstrated the utmost importance of a self-induced periodic dc-polarization linked to a third-order process mixing the fundamental and the harmonic waves, allowing for possible dipole orientation and phase matching conditions.[90]

In the same period, Ouelette et al. have reported the erasure of such self-organized $\chi^{(2)}$ gratings in optically poled fiber by ultra-violet irradiation or strong green light. The origin of the second order response was explained by the presence of periodic domains in which charge separation have occurred and charge defects trapped, as concluded by the time dependence of the erasure process.[91] This conclusion regarding the electro-optical origin of the second order optical response were confirmed by Mizrahi et al. by studying the SHG polarization properties in optically poled Ge-doped silica glass optical fiber. [92]

Similarly, Driscoll et al. have demonstrated on optically poled bulk silicate glasses that the symmetry and tensor components of the SHG response were consistent with a periodic implementation of an internal dc electric field interacting with the third-order nonlinearity, $\chi^{(3)}$, through and Electric field Induced Second Harmonic effect (EFISH).[93]

In addition, using chemical attack by hydrofluoric acid, Margullis et al. and Kyung et al., have recorded direct images of the periodic gratings resulting from macroscopic separation of charge

in the silicate glass matrix. The charge separation was mainly located at the core-clad interface of the optically poled fiber. [94] [95]

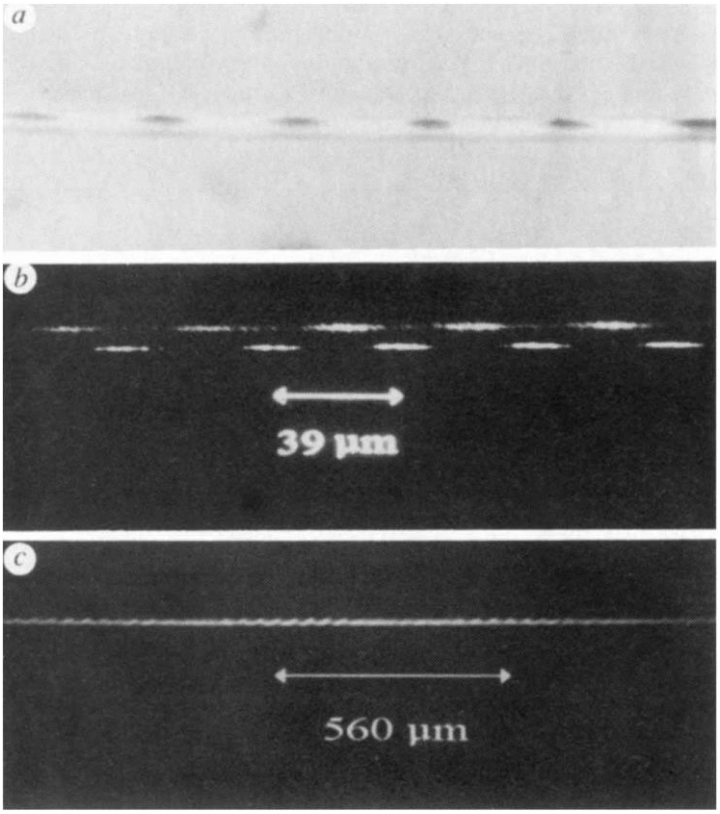

Figure 16: Second-order nonlinear gratings in frequency-doubling fibers revealed by chemical attack and observed using a phase-contrast microscope [94]

Later, the research activity on optically poled silicate glasses has significantly decreased. The mechanisms involved have been well described experimentally and theoretically, but both the low stability and effectiveness of the second order optical response induced are certainly the main reasons of this loss of interest by the community.

6.2 Three dimensional optical poling by femtosecond laser irradiation

Laser induced crystallization of second order nonlinear crystal have been developed by various several research teams. Homna et al. and Komatsu et al. have developed an approach allowing local crystal precipitation by the incorporation in the glass composition of transition or rare earth ions absorbing at infrared cw laser wavelength. The selected ions exhibit a strong non-radiative relaxation which induces an increase of the glass local temperature above the glass transition temperature and the precipitation of the second order nonlinear crystal. Nonlinear optical crystals such as β- BaB_2O_4, $Ba_2TiGe_2O_8$, $Sm_xBi_{1-x}BO_3$, (Sr, Ba)Nb_2O_6 and $LiNbO_3$ crystal have been obtained in borate, tellurate, phosphate, or silicate based glass system. [96]

Femtosecond laser irradiation is a promising tool in achieving second order nonlinear optical functionality in glasses with three-dimensional and sub-micrometer spatial resolution when no element is introduced in the glass matrix for sensitization. Two main approaches have been studied to achieve nonlinear optical functionality structuring in glasses by femtosecond laser irradiation. Several authors have reported on a three dimensional control of the precipitation of nonlinear optical crystalline phases within a glassy matrix. [97] [98] At certain high repetition rates (e.g. >200 kHz), thermal accumulation effects occur, within the irradiated volume and reach the melting temperature of the glass matrix, allowing for the crystalline phase formation. In addition, by adjusting the femtosecond laser irradiation parameters, such as writing direction and speed, pulse energy and polarization state of the light, it is possible to control the crystalline growth, and notably its orientation.[99] Finally, the objective of this laser-structuring method is to produce optical-quality single-crystal structures suitable for waveguiding. As an example we depict in Figure 17, some promising results reported on direct laser-writing of ferroelectric $LaBGeO_5$ single-crystal waveguide in a glass matrix of the same composition.

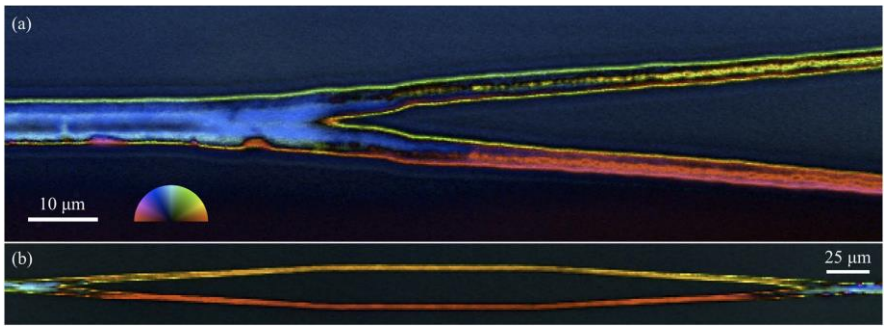

Figure 17: birefringence micrographs of crystal junctions written inside a $LaBGeO_5$ glass by femtosecond laser showing a) independent lattice orientations developed in each branch, b)the merging of the two branches back to a single line. The angle of either the fast or slow axis of birefringence is indicated by the color wheel. [98]

The second approach for femtosecond laser writing in glasses of 3D optical second-order nonlinear microstructures is linked to the use of photosensitive glasses, as reported for the first time by Choi et al.[100] As compared to the previous approach, the irradiation process does not modify the glassy state of the optical material treated. The photosensitive glasses studied were zinc phosphate glasses containing few mol% of silver oxide. Such structuring of silver containing phosphate glass needs high repetition rate and near infrared femtosecond laser sources. Careful polarization dependent SHG characterizations have demonstrated the EFISH origin of the second order optical response. The second order nonlinearity efficiency was evaluated about 2.5 times the quartz value.

One particularity concerns the fact that the inscribing of the nonlinear optical response is achieved together with the creation of silver ionic clusters exhibiting strong visible luminescence. [101] The formation mechanisms of both SHG response and silver clusters within the glass matrix by femtosecond laser irradiation involves a multi photon absorption leading to generation of free electrons, electron diffusion, and trapping but also to ionic motion

forming (i) a silver depletion at the center and (ii) silver ionic clusters at the border of the of the voxel of interaction.

For one single line inscribed by a sample translation during the irradiation, the original spatial distribution of the nonlinear pattern is composed of four lines, two lines at each side of the beam voxel (Figure 18). By SHG/luminescence correlative microscopy the locations of fluorescent and SHG signals have been characterized (see Figure 18). On the base of the EFISH origin of the signal, the electric field and electric potential distributions have been estimated. It has allowed to point out a clear correlation between the electric potential of the induced space charge and the formation and stabilization of the luminescent silver clusters. Finally the SHG lines are explained by the two electric field components of opposite sign as shown in Figure 18b.

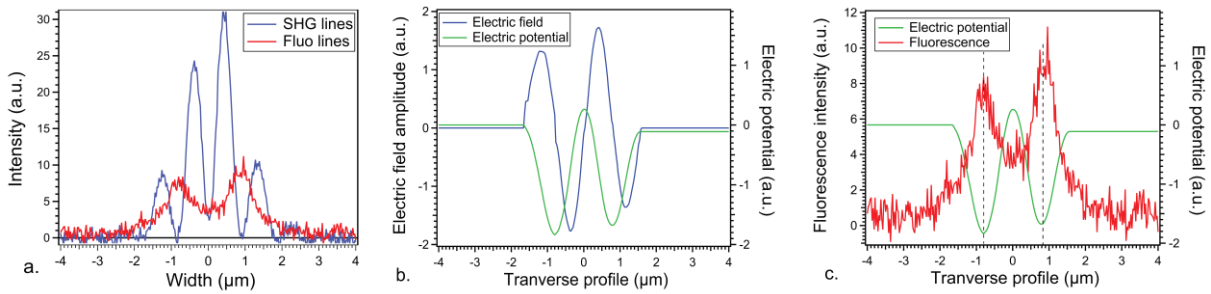

Figure 18: (a) Spatial distributions of the fluorescence and SHG signal induced after femtosecond irradiation of photosensitive silver doped phosphate glass. (b) Electric field and potential profiles deduced from the EFISH origin of the second order optical non linearity. (c) Correlation between the calculated electrical potential and the fluorescence signal originating from the silver cluster stabilized within the glass matrix. [102]

Remarkably, the second harmonic generation signal has been foundstable for temperature close to the glass transition temperature. [101]

6.3 Second order optical response in glasses by thermal electrical poling.

A thermal electrical poling procedure consists of applying a DC electric field at the sample to an elevated temperature, before cooling while the DC field is kept on (Figure 19). Such a simple process was largely studied to induce second order optical response in polymers and inorganic glasses. If one focus on thermally poled glasses, research efforts from both physics and glass chemistry communities. This interdisciplinary approach of the problem has demonstrated the potential but also the restriction and the complexity of polarization processes in a large range of glassy systems. It has contributed to demonstrate the creation of a mobile cation depleted zone under the anode side (Figure 19)

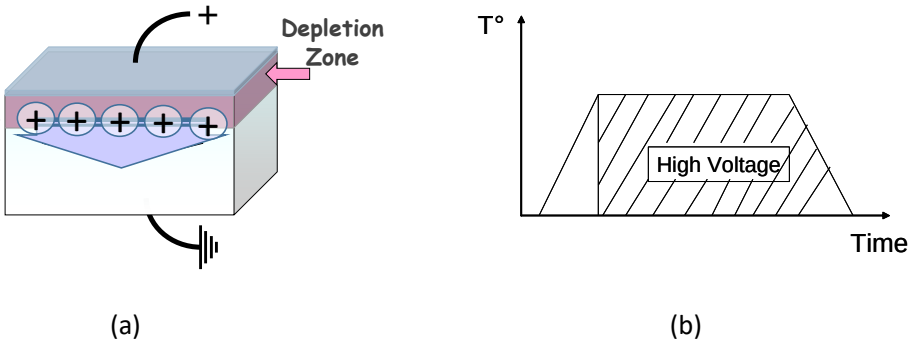

Figure 19 : thermal electrical poling of glass : (a) formation of a mobile cation depleted zone during the poling (b) description of the procedure of poling corresponding to the application of a DC electric field during heat treatment and its preservation during cooling.

The next sections will treat separately the achievements reported on silica, ionic and non-oxide glasses.

6.3.1 Thermally poled silica

SHG response in thermally poled glasses was reported for the first time by Myers et al. in 1991.[85] A $\chi^{(2)}$ response of 1pm/V was measured and related to two possible origins as expressed in Equ. 18: [103]

$$\chi^{(2)} \approx 3\chi^{(3)}.E_{dc} + \frac{Np\beta}{5k_bT}.E_{loc} \qquad (18)$$

The first term is connected to the existence of a static electric fields (E_{dc}) frozen within the sample after poling and a coupling with the intrinsic third order susceptibility $\chi^{(3)}$ of the glass matrix. This is considered as an electric field–induced second harmonic (EFISH) response linked to a space charge within the glass. The second term corresponds to the contribution of an oriented structure, which was approximated by oriented dipole where N is the number of dipoles per volume, p is the dipole moment, β the microscopic hyperpolarizability and E_{loc} corresponds to the local electromagnetic field. At the same time, Kazansky et al. have demonstrated that the origin of SONL properties in thermally poled silica is due to an EFISH process by characterizing the relative values of the nonlinear tensor components.[104]

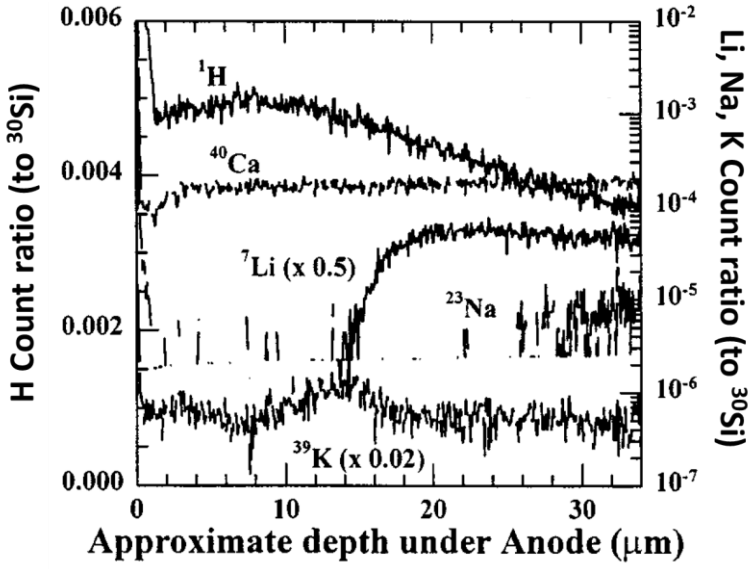

Figure 20: SIMS characterization of the alkaline depletion layers at the anode side of a silica plate poled for a duration of 140 min. [105]

The depletion zone in mobile cations at the origin of the space charge implementation were observed experimentally for the first time by SIMS (Secondary Ion Mass Spectrometry) by Alley et. al [105] As shown in Figure 20, they have observed the depletions of lithium and sodium cations over thicknesses of 17 and 25 µm respectively. In the same report, these values were shown to be dependent of the poling time. Several studies have characterized both the second order optical response efficiency and the thickness of the SHG-active layer as a function of the treatment conditions (Temperature, voltage, duration, atmosphere). [106] [107] [108] [109] [110] [111]

Polarization mechanisms in poled silica have been described by Quiquempois et al., who developed a model taking into account charge dissociation and charge recombination occurring during the poling process [112] . This description is based on the model first developed by Proctor and Sutton in 1959. It predicts the electric field distribution and a poling voltage threshold.[113] Experimental observations are in good accordance with the model. . Finally, poling mechanisms in silica are well described by a competition between charge dissociation and charge recombination leading to the appearance of a voltage threshold above which the internal electric field can be implemented.

Nevertheless, depending on the type of silica (purity, fabrication process..) , differences up to two orders of magnitude have been reported for second order optical efficiency.[114]

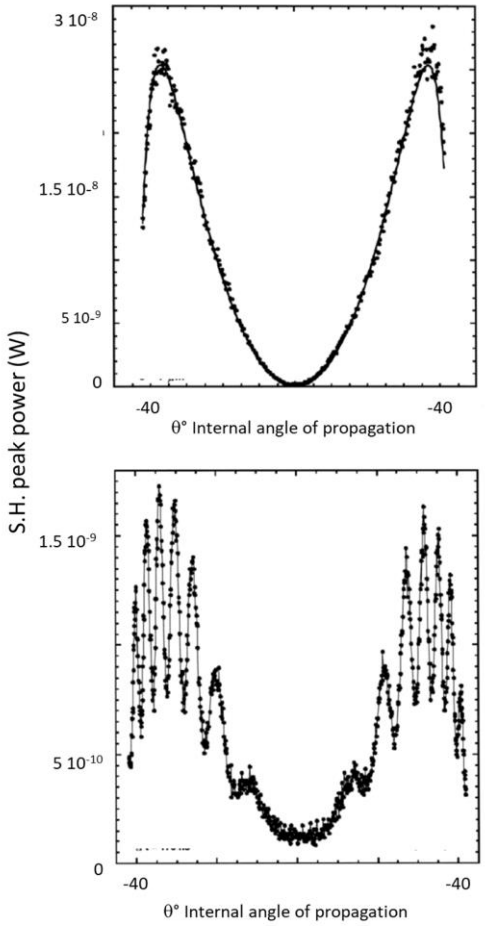

Figure 21: Second Harmonic Generation Maker fringes patterns measured for infrasil (top) and suprasil (down) poled silica types.[114]

As an example, Figure 21 compares the SHG efficiency measured for two poled silica (infrasil and suprasil) using the Maker Fringes Technique. Such technique simply consists to measure the SHG signal in transmission as a function of the angle of incidence between the incident laser and the sample. The rotation of the sample permits to induce a change of the optical path inducing the observation of interference fringes. In Figure 21, the two poled silica plates exhibit completely different SHG patterns mainly due to differences in the thickness of the SHG active

layer but the key point concerns the SHG efficiency showing a difference greater than one order of magnitude. It is now believed that the SONL efficiency is highly dependent on the initial glass composition and notably the amount of both mobile alkali cations and hydroxyl impurities. The best result were obtained for the Infrasil® silica type with alkaline content (Na^+, Li^+, K^+) in the order of few ppm. [115]

6.3.2 Optical devices based on thermally poled silica based glass

Planar devices

As opposed to natural birefringent crystalline materials like the standard KDP (KH_2PO_4) and BBO (BaB_2O_4) used for frequency conversion, phase matching conditions cannot be achieved in thermally poled glasses. Nevertheless, quasi-phase-matching (QPM) conditions are possible if a spatial distribution of the induced electric field can be inscribed in the material. The principal methodologies used to spatially structure the embedded electric field in thermally poled silica are based either on a local erasure of a macroscopic poled surface or on the use of periodic electrodes. As the coherence length of silica is rather large (in the order of 30–40 μm for an harmonic wave at 532 nm), the spatial resolution needed to obtain QPM condition can be reached quite easily by the use of classical lithography methods for example to fabricate either masks or periodic electrodes.

We will focus now on some devices designed from poled silica based planar waveguides, on their performances and on the fabrication methods. Chao et al. have polarized planar waveguide (14 mm of length) fabricated from a silica glass film doped with germanium oxide. Aluminum masks and a 266 nm UV light exposure (4-6 ns pulse width and 8 mJ pulse power) were used for a local erasure of the implemented static electric field. The low second order non linearity achieved ($\chi^{(2)}_{eff}$ = 0.03 pm/V) limits the conversion efficiency of this particular device. [116]

Similarly, a second-order nonlinear grating has been fabricated using uniform thermal poling followed by periodic erasure inside an e-beam deposition. Nevertheless, the overall performance of this device remains insufficient with a very low effective nonlinear coefficient of 0.0075 pm/V. [117]

Fage-Pedersen et al. have obtained the best results so far with SiO_2 films using periodical electrodes. A precise control of the quasi-phase-matching wavelength and bandwidth were observed thanks to a high periodic contrast of the nonlinearity with an effective $\chi^{(2)}$ of 0.13 pm/V. [118] The same authors have related the good performance of their device to the use of encapsulated periodic electrodes positioned as close as possible to the core layer (Figure 22).[119]

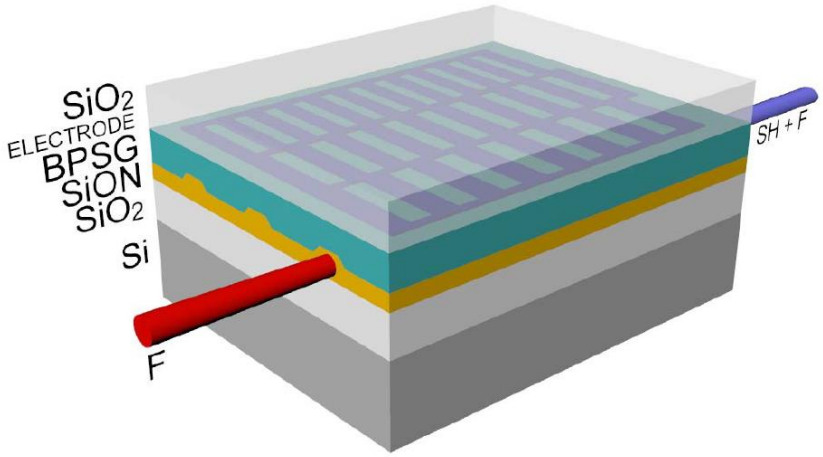

Figure 22: Schematic of a device containing three waveguides with different quasi phase matching periods. [118]

Thermally poled optical fibers

To compensate the intrinsically low nonlinear coefficient of poled silica, electro-optical modulators or frequency convertors have been also developed using poled silica glass fibers, with the idea to increase the light path length. Two methods have been tested to apply a thermal

electrical poling treatment to optical fibers: (i) using a D-shaped fiber on which a periodical electrode can be applied [120] [121] or (ii) by incorporating two electrodes within a twin-hole fiber.[122] [123]

Using the first approach, an efficient frequency doubling of 20% has been reported, but rather limited additional results have been published to confirm this performance.

By designing composite optical fibers with embedded electrodes several electro-optical modulators were successfully designed and the poling treatment was modelled (Figure 23). Particular attention was paid to the electrode/clad geometry as well as on the electrical configuration of the treatment. It was notably found that using a two-anode configurations i.e. both internal electrodes of a twin-hole fiber at the same anodic potential resulted in strong nonlinearity comparable with the conventional bulk cases. [124] [125] [126] [127]

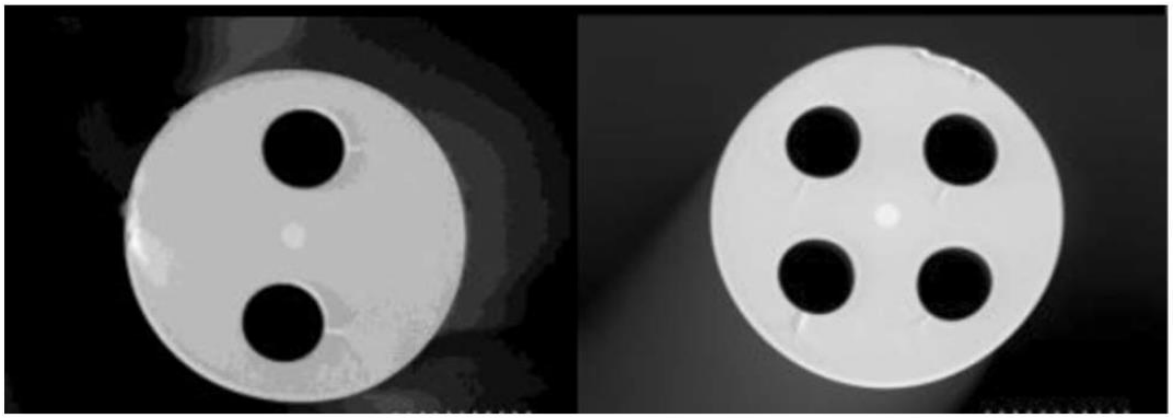

Figure 23: Example of micro structured optical fiber designed for electrical poling. In black the holes for electrode insertion and in white the core of the fiber. [128]

Finally, important technological efforts were made and are still in progress to use poled silica in photonic devices, but their use as frequency converters turns out to be limited because of the weakness of their intrinsic SONL responses.

6.3.3 Thermal poling of cation rich glasses

The pioneer works concerning electrical polarization processes of cation rich glasses were published by Carlson et al. in the 70 s,[129] [130] [131] [132] but the first report concerning SONL in thermally poled ionic glasses was published in 1998 on soda lime and borosilicate commercial glasses.[133] In these first works, it was notably demonstrated that a complete depletion of mobile cations can be formed at the anode side of the poled ionic glass which involves a very large displacement of mater and significant composition variations. Within this depletion layer, large SONL responses have been observed for a large variety of oxide glasses such as silicate, borate, phosphate and germanate.[134] [135] [136] [137] [138] [139] [140] As an example, a $\chi^{(2)}$ up to 5 pm/V was obtained on a sodium niobium borophosphate (see Figure 24)

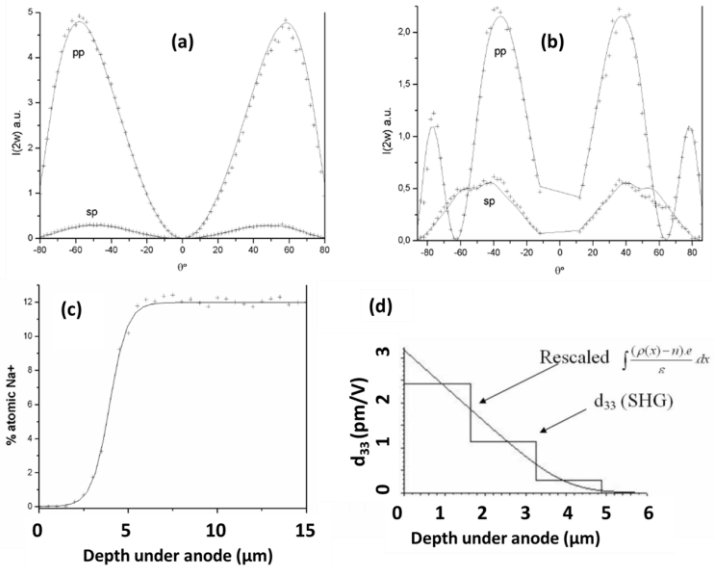

Figure 24: Maker fringes analysis performed on a thermally poled sodium niobium borophosphate glass in transmission (a) and reflection (b) mode. The experimental data are shown with crosses, the simulation with a line. (c) Depth profile of the sodium concentration measured at the anode side of the poled sample, showing a complete depletion of 12 mol% of

Na^+ cations. (d) Depth profiles comparison of (i) the SONL active layer calculated from the Maker fringes analysis and (ii) the static electric field implemented estimated from the sodium depletion data.[141]

Polarization mechanisms in cation rich oxide glasses and SONL

As shown in the previous example, the complete charge dissociation process occurring during a thermal poling treatment involves large displacements of mobile cations towards the cathode. To counterpart this cation departure, two main compensation processes have been proposed. First, most authors have agreed on the role of protonic species injection from air, which could be described as an ion-exchange process driven by electric field and corresponding to an open anode poling configuration. Second, if one considers a blocking anode, the conductivity of negative charge carriers, involving large structural rearrangements, have to be considered. In order to describe the relative influence of these two compensation mechanisms in cationic glasses, an important number of studies have concerned the influence of the treatment atmosphere on the structural rearrangements within the glass matrix. [142] [143] [139] [144]

Two examples of this methodologic approach, combining a state of the art correlative technique combining Raman spectroscopy and SHG microscopy is shown in Figures 25 and 26. The Raman maps show the different structural rearangment attributed to the two main compensation mechanisms for the cation depletion which is the hydroxyls injection and the network reticulation that can lead to the formation of molecular oxygen as shown respectively in Figure 25 A, B, C for silicate and in Figure 26 for a sodium germano-niobate oxide glass. This modified layer at the anode side can be easily correlated to the space charge location using second harmonic generation maping (Figure 25D).

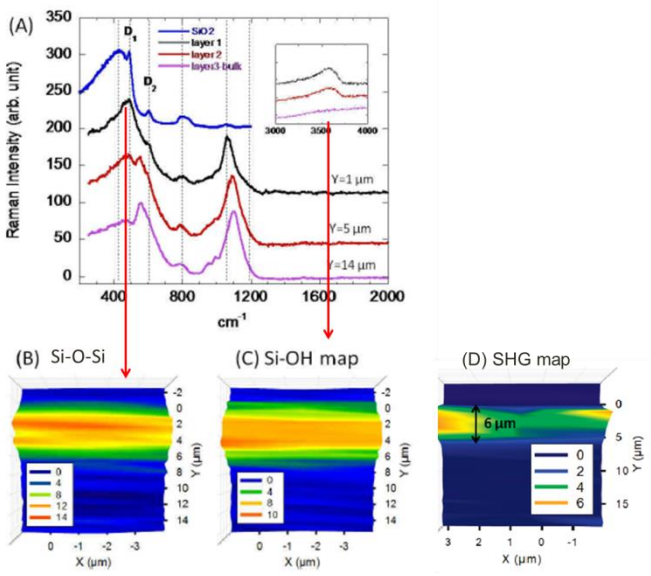

Figure 25: (A) Raman spectra measured from the anode surface towards the bulk of a poled soda lime glass. The silica spectra is shown as a reference for the spectral assignments. (B) and (C) are Raman mapping showing (i) the reticulation of the silicate network and (ii) the injection of hydroxyl group. (D) is the SHG image measured within the same exact zone. [145]

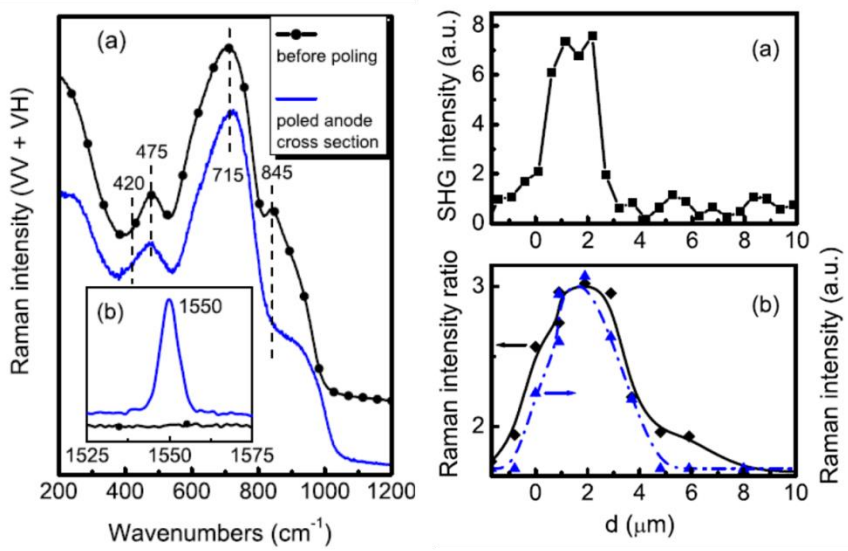

Fig 26: Example of correlated SHG /Raman study done on a sodium germano-niobate oxide glass. Left part: it is depicted the spectral variations induced at the anode side of the glass and

notably the occurrence of a band 1550 cm^{-1} linked to the formation of molecular oxygen within the glass matrix. Right part: spatial correlation between location of the SONL response (a) and the structural rearrangements (b). In the Raman profile part of the figure, triangles (blue dashed curve) are linked to the intensity of the Raman band 1550 cm^{-1}, lozenges (black full curve) correspond to the intensity ratio of the bands at 715 and 845 cm^{-1}. [138]

The nature of the negative charge carriers involved during the poling process to compensate the cation depletion is a complex problem which has been the subject of several studies. The respective roles of electronic and/or anionic contributions have notably been discussed on the base of a large range of experimental data.[146] [147] [148] [149] [150] [140] [151] [152]

Recently, a new description of these compensations mechanisms has been proposed. In the case of a semi-blocking anode, Redox reactivity between different positive and negative charge carriers has been proposed to explain the observation of nitrogen oxide molecular species trapped within the polarized glassy matrix by Raman spectroscopy. Second, for a blocking anode configuration, the mechanism proposed by Redkov et al. for a silicate glass describes an electronic conductivity involving (i) peroxide radical formation during the charge dissociation mechanism and (ii) their reactivity to form the new glass structure and trapped molecular oxygen.[153] [154] [155]

Finally, as the strength of the internal electric field implemented controls the SONL efficiency, one should definitely focus on the influence of the mechanisms compensating the formation of the cation depletion. That was notably shown by comparing the $\chi^{(2)}$ values obtained for two poling treatment of a soda lime glass done in argon or in air atmosphere. The blocking electrode configuration, (no charge injection within the glass matrix at the anode-poling under argon),

allows the generation of a SONL response ten times higher than the poling done in air, promoting protonic injections.[115] The EFISH origin of SHG signal was confirmed by careful Maker fringes analysis and modeling. The internal electric field strength was estimated to 3.10^8 V/m for the argon-poled soda lime glass. This value is similar to the one estimated for the Infrasil silica poled sample. It proves that, if the poling procedure prevents any charge injection from the atmosphere, it is possible in a cation-rich silicate glass to achieve the implementation of an internal electric field as strong as that for poled silica. At the opposite, if the hydroxyl group injection is predominant, and the space charge can be almost totally compensated.

6.3.4 $\chi^{(2)}$ structuring in cation rich glasses

Regarding thermal electric treatment and cation rich glasses, the main advantage is linked to the possibility to use the poling process as an imprinting approach by the use of structured electrode. Such an imprinting process was notably reported for sub-micrometer scale structuring of surface relief [156] [157] and linear optical properties. One example is given in Figure 27 in which the topology profile of the electrode, used as a stamp during the poling process, is compared to the poled glass relief after treatment. This process has been linked to changes of the glass composition inducing density modifications and mechanical constrains governed by the electrode design .The validity of the method was demonstrated by the fabrication of diffraction grating.[158] [159] [160] [161] [162]

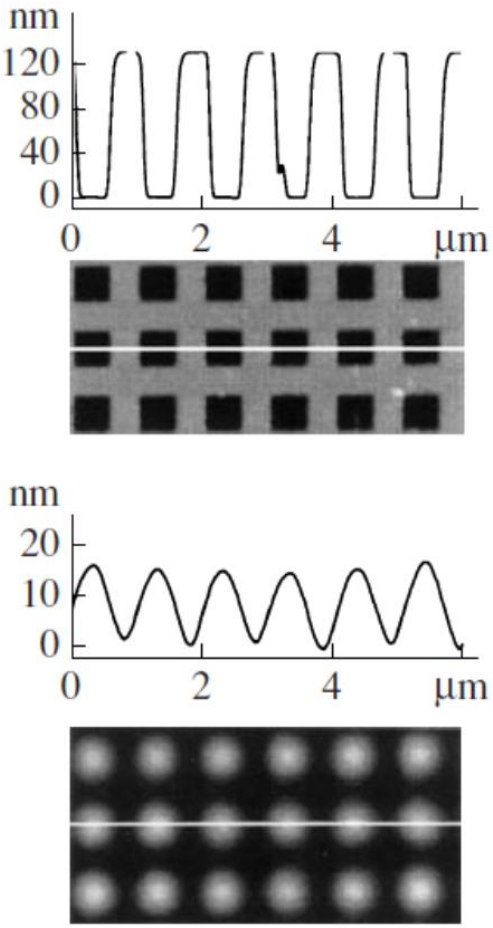

Figure 27: Topology picture and profiles of (i) the structured anode (up) and (ii) the polarized soda lime glass surface (down). [163]

In addition, a few reports exist on the use of this kind of imprinting process for structuring SONL response.[164] [165] Using micro-patterned silicon substrates, micro-structured second harmonic generation responses have been achieved on sodium-phospho niobate glasses. Sub-micrometer sized patterns of both surface relief and second order optical responses were fabricated on the anode glass surface. The authors have pointed out that in their poling conditions the patterns do not simply follow the electrical potential expected from the anode topology.[166] The possibility of field enhancement effects within the micro structured electrode is proposed to play a key role to govern the charge density on the glass surface during

the process. This could finally control the amplitudes of both implemented static electric field for the SONL response and Maxwell stresses for the topology.

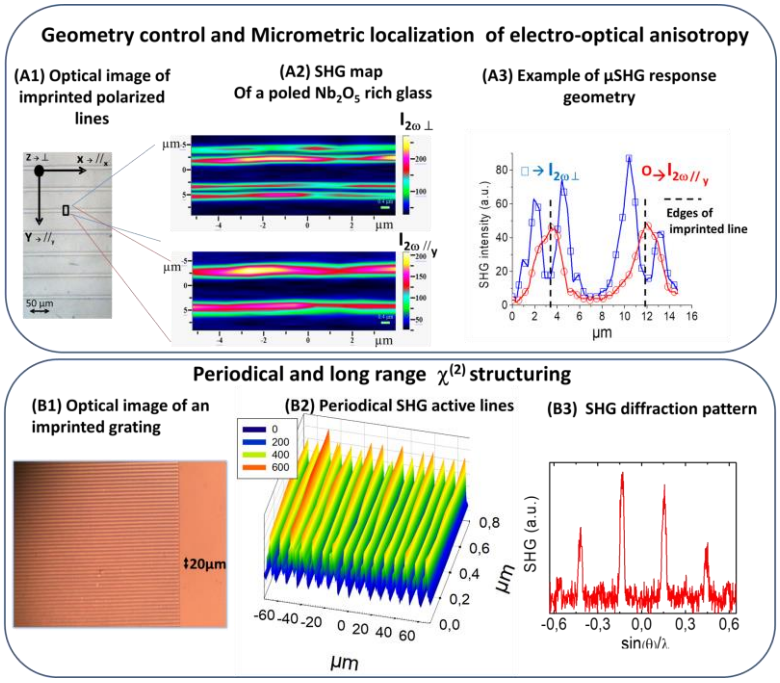

Figure 28: (upper part) (A1) Optical image of the surface of glass after a thermal poling imprinting process. (A2 and A3) Longitudinal and in plane SHG signal measured for one imprinted line. (lower part) (B1) Optical image of an imprinted grating and (B2) the SHG response of the gratting measured in microscopy. (B3) SHG diffraction pattern measured for this 4mm^2 sized grating. [165]

A more advanced set of results have recently shown that this kind of imprinting process allows for spatial and geometry controls of second order optical properties at the micrometer scale.[165] As shown in the upper part of Figure 28, the geometry of the optical anisotropy was characterized by SHG microscopy using radial or azimuthal polarization state of the incident laser to probe the respective longitudinal and in plane components: (i) at each boarder of the electrode, the SHG response is two orders of magnitude higher and (ii) one in plane component

is localized in between two longitudinal components (Figure 28 A2 and A3) A simple electrostatic model taking in account local field enhancement, and lateral poling effects allows reproducing the experimental data. It denotes that a control of the location and the geometry of the electro-optical anisotropy can be obtained. As it can be described by simple electrostatic models, it opens the way to accurate designs of SONL response in glass by managing electric field distribution on micro-structured electrodes.

The potential of such a process to fabricate large-scale micro-structured periodical design of second order optical properties has been demonstrated.[165] [164] The example given in Figure 28 (lower part) is a SHG-grating inscribed by poling on phospho niobate bulk glass. The period of the SONL pattern is 5µm on a surface of several mm^2. The micrometric dimension of the pattern as well as the long range periodicity was confirmed by SHG microscopy (Figure 28 B2) and SHG diffraction (Figure 28 B3) measurements respectively.

6.3.3 SONL in thermally poled chalcogenide glasses

Considering a possible use of poled glasses in photonic devices, the two main issues to be targeted are (i) an increase of the efficiency of the second order optical response and (ii) ensuring a real temporal stability. If one consider an EFISH origin of the non-linearity, as the magnitude of the static electric field cannot be increased in classical oxide glassy systems, high $\chi^{(3)}$ glasses should be considered to improve poling induced $\chi^{(2)}$ values (see Eq. 18)

Chalcogenide amorphous materials are based on chalcogens (S, Se, and Te) covalently bound to other suitable elements like Ge, As, Sb used as network formers. These glasses are well-known for their high third-order susceptibility $\chi^{(3)}$ which can be a thousand time larger than that in silica glass (Figure 5 part 5.1). Thus, Chalcogenide glasses can be considered as potential candidates to generate, after a thermal poling treatment, large second order susceptibility which theoretically could compete with highly nonlinear single crystals in optical devices.[167] [168]

[169] [21] [24] [10] [170] [171] In addition, their large domain of transparency opens up unique possibilities for the development of new devices for promising applications of parametric frequency converters and electro-optic modulators in the IR spectral region.

One should notice that in the literature, SONL induced by thermal poling in chalcogenide have been studied only for sulphide compositions and mainly for germanium- or arsenic-based sulphide glasses[172] because of their transparency in visible and near-IR allowing second harmonic generation measurements from near-IR and mid-IR laser sources, which is not possible for selenide or telluride glasses.

Guignard et al. were the first to report strong second-order coefficients, $\chi^{(2)}$, up to 8 pm/V for a $Ge_{25}Sb_{10}S_{65}$ thermally poled glass.[172] This value was obtained using a simulation based on the accurate knowledge of the thickness of the nonlinear layer, ensuring the reliability of the quantitative measurement. In addition, the performance of the same glass system was found to be significantly increased by femtosecond laser irradiation.[173] The highest $\chi^{(2)}$ value was found to be 11.4 pm/V, 40-50% larger than before laser exposure. Raman spectral changes seem to indicate that defects were created, enhancing the third-order optical nonlinearity of the glass, and as a result its second-order nonlinearity. Large SHG efficiency was also shown in chalcohalide glassy systems. The compositions 0.56GeS2–0.24Ga2S3–0.2KI and 60GeS2–20Ga2S3–20KBr were studied by Jing et al. [174] and for an optimized thermal poling process (5.2 kV, 260 °C for 120 min), the coefficient $\chi^{(2)}$ was as strong as 3.74 pm/V. Dong et al. have worked on a similar system but modified by silver chloride: (100-x)(80GeS2-20Ga2S3)-xAgCl.[175] The polarization of the glass was achieved by irradiation with an electron beam with moderate energy (25 kV, 25nA, 15 min). The SHG intensity of the irradiated glass is assumed to be about 1.5 times larger than that of Z-cut quartz as a reference, and the $\chi^{(2)}$ is estimated to be greater than 6.1pm/V.

These different reports clearly demonstrate that large second order optical response can be achieved in thermally poled chalcogenide glasses. However, these studies have also shown the restriction due to the low temporal stability of the poling effects in these glass systems which reiterates the need for an accurate description of the poling mechanisms for these compositions.[176]

Guignard et al. have compared poling current and SONL response as a function of the treatment duration, temperature, and voltage for two sulfur germanate systems with or without gallium.[172] SHG signals were generated within the first 15 micrometres under the anode side in both glasses for different optimised poling parameters. Two distinct behaviours were clearly observed upon poling. For the gallium containing glasses, the poling current slightly increase during the treatment and the SHG signal increases continuously with the increase of the poling temperature until the appearance of damage. Without gallium in the Ge-S based glasses, the poling current exhibits a severe decrease from about ten to few µA and the second order nonlinear susceptibility is maximal for a poling time of few minutes at about 170°C. (Figure 29)

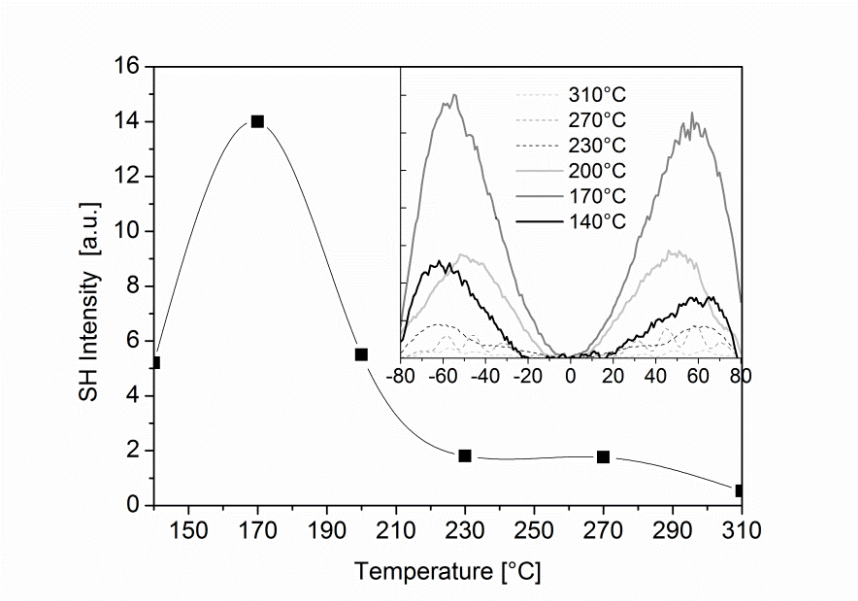

Figure 29: Maximum SH intensity versus the temperature used for the poling process of $Ge_{25}Sb_{10}S_{65}$ glass and MF patterns recorded for different temperatures from 170°C to 310°C. [172]

These behavior variations upon poling were linked to a higher electronic conductivity in gallium-containing glasses and two mechanisms were proposed to explain the creation of a nonlinear layer under the anodic surface. The formation and migration of charged defects towards the anode was proposed for glasses containing gallium and exhibiting a higher electronic conductivity, whereas the migration of cationic species, Na^+ , which was observed by SIMS analysis, may play a more important role for of the accumulation of negative charges under the anode in germanium based sulphide glasses.

In a similar glassy system, Gu et al. proposed that the mechanism of SHG in GeS_2-Ga_2S_3-CdS glasses is related to the reorientation of dipoles originated from the structural defects within the glasses. Under given poling conditions (5 kV, 280°C, 30 min), differences of $\chi^{(2)}$ efficiency as a function of the composition are proposed to be due to changes of dipole reorientation ability with the evolution of glassy structure. [177]

Considering arsenic-based glasses, the creation of a second order nonlinearity has been firstly achieved by using thermal-electric but also optically assisted poling treatments of As_2S_3 chalcogenide thin film.[178] The As_2S_3 amorphous films of about 4 µm were deposited onto an indium tin oxide transparent thin electrode on a BK7 substrate. The $\chi^{(2)}$ coefficient was estimated to be greater than 0.6 pm/V whatever the used poling method. It is worth mentioning that high photosensitivity was observed induced by near bandgap illumination (488 and 514nm, 5J/mm2, and 2.5mW/mm2) which have influenced considerably the SONL efficiency and stability. More accurate studies of the links between (i) alkali content of chalcogenide glass

compositions, (ii) photosensitivity and (iii) thermal poling induced SONL stability have been reported.[179] [180] Careful Raman and SHG signal characterizations were carried out in order to improve the understanding of SONL stability of poled chalcogenides. The discussion was based on the nature of trapped charges within the glass matrix and rationalized in agreement with the model proposed by Shimakawa.[181] [182] For a non-doped As_2S_3 glass, the displacement of positive charges is four orders of magnitude lower than the Na^+-doped composition. The space formation is thus mainly formed by charged defects also called Self-Trapped Excitons, which are not stable in time and accelerate the creation of structural rearrangements upon light irradiation. On the other hand, for the Na^+-doped As_2S_3 compositions, the electrical current during the poling treatment is non negligible and the formation of trapped charges is accompanied by structural rearrangements. Such trapped charges are called Random Pairs, the SONL responses are founded stable, and the photosensitivity within the space charge layer is almost totally reduced.

As an example, in a germano-arsenic composition the poling induced SHG response was founded to decrease rapidly in few minutes whereas the same glass doped with 1 mol% of sodium, shows a stable response for more than a year (Figure 30).

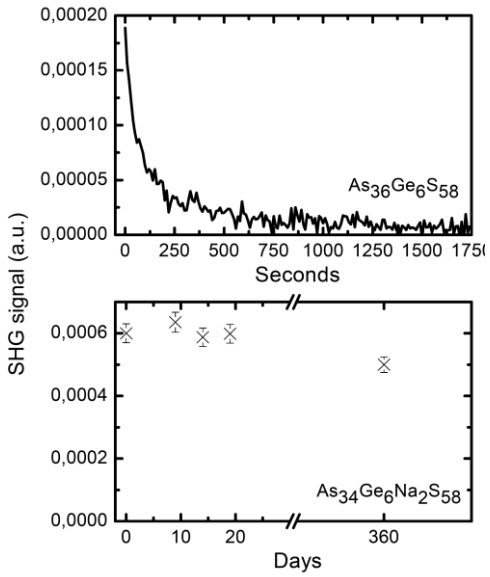

Figure. 30: Kinetics of SHG signal stability for poled glasses of compositions $As_{36}Ge_6S_{58}$ (top) $As_{34}Ge_6Na_2S_{58}$ (bottom).[179]

These studies on thermal electrical poling in chalcogenides have demonstrated the importance of a rearrangement of the glass matrix induced by the polarization treatment in order to stabilize the SONL properties. Nevertheless, the $\chi^{(2)}$ values achieved in these stable poled chalcogenides are very low, on the order of 5.10^{-2} pm/V. This leads to an estimate of the static field strength on the order of few 10^4 V/m which is four order of magnitude lower than that for oxide glasses. Both explanations of (i) low value of optical nonlinearity and (ii) low stability for effective polarized chalcogenide glasses should be linked to the electronic conductivity of these glasses. It opens the route for glass chemist to prepare compositions which could have limited electronic conductivity to optimize the second order optical susceptibility induced by thermal electrical poling in such promising glassy systems.

7. Conclusion

In the last 30 years, the development of lasers, glass science and associated technologies has allowed taking advantage of numerous nonlinear optical properties of glass. Investigations have concerned the fundamental aspects of the glass response, but also innovative technologies for exploiting nonlinear optical phenomena and bring them to practical life. These discoveries are at the base of the information technologies and invade nowadays sectors such as security or health. In terms of materials, even if silica or silicate based materials exhibit often low nonlinear optical response, the extremely low loss achieved in this materials has allowed the exploitation of nonlinear optical phenomena using often long distance propagation. New compositions could allow reductions in the size of optical systems thanks to high nonlinear optical performance if high optical quality materials can be optimized and developed, as demonstrated in recent years.

Acknowledgement

The authors gratefully acknowledge Pr. Canioni and Dr. Royon for their help to setup this chapter.

This study has been carried out with financial support from the French State, managed by the French National Research Agency (ANR) in the frame of "the Investments for the future" Programme IdEx Bordeaux—LAPHIA (ANR-10-IDEX-03-02)

References

[1] T. H. Maiman: Simulated Optical Radiation in Ruby, Nature **187** 493 (1960).

[2] P. P. Franken, A. E. Hill, C. W. Peters, G. Weinreich: Generation of Optical Harmonics, Phys Rev. Letters **7** (4) 118 (1961).

[3] P. W. S. S. R. friberg: Nonlinear optical glasses for ultrafast optical switches IEEE J. Quantum Electron. **23** (12) 2089 (1987).

[4] E. M. Vogel, M. J. Weber, D. M. Krol: Nonlinear optical phenomena in glass, Phys Chem. Glasses **32** (6) 231 (1991).

[5] H. A. Lorentz: In Theory of electrons and its applications to the phenomena of light and radiant heat, Stechert (1909).

[6] D. A. Kleinman: Nonlinear Dielectric Polarization in Optical Media, Phys. Rev. **126** 1977 (1962).

[7] P. N. Butcher, D. Cotter: The elements of Nonlinear optics, Cambridge studies in modern optics : 9, Ed. P.L. Knight, W.J. Firth, Cambridge University Press (1990).

[8] I. Kang, S. Smolorz, T. Krauss, F. Wise, B. G. Aitken, N. F. Borelli: Time-domain observation of nuclear contributions to the optical nonlinearities of glasses, Physical review B **54** (18) 12641 (1996).

[9] M. Sheik-Bahae, D. J. Hagan, E. W. V. Stryland: Dispersion and band-gap scaling of the electronic Kerr effect in solids associated with two-photon absorption, Physical Review Letters **65** (1) 96 (1990).

[10] J. M. Harbold, F. O. Ilday, F. W. Wise, J. S. Sanghera, V. Q. Nguyen, L. B. Shaw, I. D. Aggarwal: Highly nonlinear As-S-Se glasses for all-optical switching, Opt. Lett. **27** (2) 119 (2002).

[11] H. Nasu, O. Sugimoto, J. Matsuoka, K. Kamiya: Non-resonant-type third-order optical non-linearity of alkali silicate and alkali aluminosilicate glasses — contribution of

individual chemical species in the glasses to χ(3), Journal of Non-Crystalline Solids **182** 321 (1995).

[12] T. Cardinal, E. Fargin, G. L. Flem, M. Couzi, L. Canioni, P. Segonds, L. Sarger, A. Ducasse, F. Adamietz: Nonlinear optical properties of some niobium(V) oxide glasses, Eur. J. of Solid State and Inorg. Chem **33** 597 (1996).

[13] R. A. H. El-Mallawany: Tellurite Glasses Handbook, ed. CRC Press, Boca Raton, Florida (2001).

[14] S. Suehara, P. Thomas, A. P. Mirgorodsky, T. Merle-Méjean, J. C. Champarnaud-Mesjard, T. Aizawa, S. Hishita, S. Todoroki, T. Konishi, S. Inoue: Localized hyperpolarizability approach to the origin of nonlinear optical properties in TeO2-based materials

Phys. Rev. B **70** 205121 (2004).

[15] A. P. Mirgorodsky, M. Soulis, P. Thomas, T. Merle-Méjean, M. Smirnov: Ab initio study of the nonlinear optical susceptibility of TeO2-based glasses, Phys. Rev. B **73** 134206 (2006).

[16] M. Dutreilh-Colas, P. Thomas, J. C. Champarnaud-Mesjard, E. Fargin: New TeO2 based glasses for nonlinear optical applications: study of the Tl2O-TeO2-Bi2O3, Tl2O-TeO2-PbO and Tl2O-TeO2-Ga2O3 systems, Physics and Chemistry of Glasses **44** 349 (2003).

[17] E. Fargin, A. Berthereau, T. Cardinal, G. L. Flem, L. Ducasse, L. Canioni, P. Segonds, L. Sarger, A. Ducasse: Optical non-linearity in oxide glasses, Journal of Non-Crystalline Solids **203** 96 (2003).

[18] B. Jeansannetas, S. Blanchandin, P. Thomas, P. Marchet, J. C. Champarnaud, T. Merle, B.Frit, V. Nazabal, E. Fargin, G. L. Flem, M. O. Martin, B. Bousquet, L. Canioni, S. L. Boiteux, P. Segonds, L. Sarger: Glass Structure and Optical Nonlinearities in Thallium(I) Tellurium(IV) Oxide Glasses, J. Solid State Chem. **146** 329 (1999).

[19] O. Noguera, T. Merle-Mejean, A. P. Mirgorodsky, P. Thomas, J. C. Champarnaud-Mesjard: Dynamics and crystal chemistry of tellurites. II. Composition- and temperature-dependence of the Raman spectra of x(Tl2O)+(1−x) Te2O glasses: evidence for a phase separation?, Journal of Physics and Chemistry of Solids **65** 981 (2004).

[20] T. Sekiya, N. Mochida, A. Ohtsuka, M. Tonokawa: Raman spectra of MO1/2single bondTeO2 (M = Li, Na, K, Rb, Cs and Tl) glasses, Journal of Non-Crystalline Solids **144** 128 (1992).

[21] T. Cardinal, K. Richardson, H. Shim, A. Schulte, R. Beatty, K. L. Foulgoc, C. Meneghini, J. F. Viens, A. Villeneuve: Non-linear optical properties of chalcogenide glasses in the system As-S-Se, Journal of Non-Crystalline Solids **257** 353 (1999).

[22] L. Petit, A. Humeau, N. Carlie, S. Cherukulappurath, G. Boudebs, K. Richardson: Nonlinear optical properties of glasses in the system Ge⁄Ga—Sb—S⁄Se, Opt. Lett. **31** (10) 1495 (2006).

[23] N. Finlayson, W. C. Banyai, C. T. Seaton, G. I. Stegeman, M. O'Neill, T. J. Cullen, C. N. Ironside: Optical nonlinearities in CdSxSe1-x-doped glass waveguides, J. Opt. Soc. Am. B **6** (4) 675 (1989).

[24] G. Lenz, J. Zimmermann: Large Kerr effect in bulk Se-based chalcogenide glasses, Opt. Lett. **25** (4) 254 (2000).

[25] R. W. Hellwarth, J. Cherlow, T.-T. Yang: Origin and frequency dependence of nonlinear optical susceptibilities of glasses, Physical Review B **11** 964 (1975).

[26] S. Smolorz, F. Wise, N. F. Borrelli: Measurement of the nonlinear optical response of optical fiber materials by use of spectrally resolved two-beam coupling, Opt. Lett. **24** 1103 (1999).

[27] R. H. Stolen, W. J. Tomlinson: Effect of the Raman part of the nonlinear refractive index on propagation of ultrashort optical pulses in fibers, J. Opt. Soc. Am. B **9** 565 (1992).

[28] S. Santran, L. Canioni, L. Sarger, T. Cardinal, E. Fargin: Precise and absolute measurements of the complex third-order optical susceptibility, J. Opt. Soc. Am. B **21** 2180 (2004).

[29] S. Montant, A. L. Calvez, E. Freysz, A. Ducasse, M. Couzi: Time-domain separation of nuclear and electronic contributions to the third-order nonlinearity in glasses, J. Opt. Soc. Am. B **15** 2802 (1998).

[30] A. Royon, L. Canioni, B. Bousquet, V. Rodriguez, M. Couzi, C. Rivero, T. Cardinal, E. Fargin, M. Richardson, K. Richardson: Strong nuclear contribution to the optical Kerr effect in niobium oxide containing glasses, Phys Rev B **75** 104207 (2007).

[31] D. Heiman, R. W. Hellwarth, D. S. Hamilton: Raman scattering and nonlinear refractive index measurements of optical glasses, J. Non-Cryst. Solids **34** 63 (1979).

[32] A. A. Lipovskii, D. K. Tagantsev, A. A. Vetrov, O. V. Yanush: Raman spectroscopy and the origin of electrooptical Kerr phenomenon in niobium alkali-silicate glasses, Opt. Mater. **21** 749 (2003).

[33] T. Cardinal, E. Fargin, G. L. Flem, S. Leboiteux: Correlations between structural properties of Nb2O5-NaPO3-Na2B4O7 glasses and non-linear optical activities, J. Non-Cryst. Solids **222** 228 (1997).

[34] C. V. Raman, K. S. Krishnan: A new type of secondary radiation, Nature **121** 501 (1928).

[35] R. H. Stolen, E. P. Ippen: Raman gain in optical waveguides, Appl. Phys. Lett. **22** (6) 276 (1973).

[36] R. Schafer, J. Jungjohann: Raman Amplification – Longer Wider, Faster, Cheaper, Compound Semiconductors **7** (2) 41 (2001).

[37] T. T. Basiev, A. A. Sobol, P. G. Zverev, L. I. Ivleva, V. V. Osiko, R. C. Powell: Raman spectroscopy of crystals for stimulated Raman scattering, Optical Materials **11** 307 (1999).

[38] E. M. Dianov: Advances in Raman Fibers, J. Lightwave Technol. **20** (8) 1457 (2002).

[39] F. L. Galeener, J. C. M. Jr., R. H. Geils, W. J. Mosby: The relative Raman cross sections of vitreous SiO2, GeO2, B2O3, and P2O5, Appl. Phys. Lett. **32** (1) 34 (1978).

[40] M. E. Lines: Absolute Raman Intensities in Glasses, I. Theory, J. Non-Cryst. Solids **89** 143 (1987).

[41] M. E. Lines, A. E. Miller, K. Nassau, K. B. Lyons: Absolute Raman Intensities in Glasses, II. Germania-based heavy metal oxides and global criteria, J. Non-Cryst. Solids **89** 163 (1987).

[42] A. E. Miller, K. Nassau, K. B. Lyons, M. E. Lines: The intensity of Raman scattering in glasses containing heavy metal oxides, J. Non-Cryst. Solids **99** 289 (1988).

[43] D. Chang, S. V. Chernikov, M. J. Guy, J. R. Taylor, H. J. Kong: Efficient cascaded Raman generation and signal amplification at 1.3 μm in GeO2-doped single mode fibre, Optics Comm. **142** 289 (1997).

[44] H. S. Seo, K. Oh: Optimization of silica fiber Raman amplifier using the Raman frequency modeling for an arbitrary GeO2 concentration, Optics Comm. **181** 145 (2000).

[45] G. A. Thomas, D. A. Ackerman, P. R. Prucnal, S. L. Cooper: Physics in the Whirlwind of Optical Communications, Physics Today **September** 30 (2000).

[46] J. Bromage, K. Rottwitt, M. E. Lines: A Method to Predict the Raman Gain Spectra of Germanosilicate Fibers With Arbitrary Index Profiles, IEEE Photon. Technol. Lett. **14** (1) 24 (2002).

[47] E. M. Dianov, M. V. Grekov, I. A. Bufetov, S. A. Vasiliev, O. I. Medvedkov, V. G. Plotnichenko, V. V, Koltashev, A. V. Belov, M. M. Bubnov, S. L. Semjonov, A. M.

Prokhorov: CW high power 1.24 μm and 1.48 μm Raman laser based on low loss phosphosilicate fibre, Electron. Lett. **33** (18) 1542 (1997).

[48] E. M. Dianov, M. V. Grekov, I. A. Bufetov, V. M. Mashinsky, O. D. Sazhin, A. M. Prokhorov, G. G. Devyatykh, A. N. Guryanov, V. F. Khopin: Highly efficient 1.3 μm Raman fibre amplifier, Electron. Lett. **34** (7) 669 (1998).

[49] Z. Pan, S. H. Morgan, B. H. Long: Raman scattering cross-sections and non-linear optical response of lead borate glasses, J. Non-Cryst. Solids **185** 127 (1995).

[50] A. Mori, H. Masuda, K. Shikano, K. Oikawa, K. Kato, M. Shimizu: Ultra-wideband tellurite-based Raman fibre amplifier, Electron. Lett. **37** (24) 1442 (2001).

[51] R. Stegeman, L. Jankovic, H. Kim, C. Rivero, G. Stegeman, K. Richardson, P. Delfyett, Y. Guo, A. Schulte, T. Cardinal: Tellurite glasses with peak absolute Raman gain coefficients up to 30 times that of fused silica, Optics Lett. **28** 1126 (2003).

[52] G. Dai, F. Tassone, A. L. Bassi, V. Russo, C. E. Bottani, F. D'Amore: TeO2-based glasses containing Nb2O5, TiO2, and WO3 for discrete Raman fiber amplification, Photon. Technol. Lett. **16** (4) 1011 (2004).

[53] V. G. Plotnichenko, V. V. Koltashev, V. O. Sokolov, E. M. Dianov, I. A. Grishin, M. F. Churbanov: Raman band intensities of tellurite glasses, Optics Lett. **30** 1156 (2005).

[54] R. Stegeman, C. Rivero, K. Richardson, G. Stegeman, P. Delfyett, Y. Guo, A. Pope, A. Schulte, T. Cardinal, P. Thomas, J.-C. Champarnaud-Mesjard: Raman gain measurements of thallium-tellurium oxide glasses, Optics Express **13** (4) 1144 (2005).

[55] G. S. Murugan, T. Suzuki, Y. Ohishi: Tellurite glasses for ultrabroadband fiber Raman amplifiers, Appl. Phys. Lett. **86** 161109 (2005).

[56] C. Rivero, K. Richardson, R. Stegeman, G. Stegeman, T. Cardinal, E. Fargin, M. Couzi: Characterization of the Performance Parameters of Some New Broadband Glasses for Raman Amplification, Journal of Glass Technology **46** (2) 80 (2005).

[57] S. Kim, T. Yoko: Nonlinear Optical Properties of TeO2-Based Glasses: MOx-TeO2 (M= Sc, Ti, V, Nb, Mo, Ta, and W) Binary Glasses, Journal of the American Ceramic Society **78** 1061 (1995).

[58] C. Rivero, R. Stegeman, K. Richardson, G. Stegeman, G. Turri, M. Bass, P. Thomas, M. Udovic, T. Cardinal, E. Fargin, M. Couzi, H. Jain, A. Miller: Influence of modifier oxides on the structural and optical properties of binary TeO2 glasses, J. Appl. Phys. **101** 023526 (2007).

[59] V. Rodriguez, G. Guery, M. Dussauze, F. Adamietz, T. Cardinal, K. Richardson: Raman Gain in Tellurite Glass: How Combination of IR, Raman, Hyper-Raman and Hyper-Rayleigh Brings New Understandings, J. Phys. Chem C **120** (40) 23144 (2016).

[60] C. Rivero, R. Stegeman, D. Talaga, M. Couzi, T. Cardinal, K. Richardson, G. Stegeman: Resolved discrepancies between visible spontaneous Raman cross-section and direct near-infrared Raman gain measurements in TeO2-based glasses, Optics Express **13** (12) 4759 (2005).

[61] M. Asobe, T. Kanamori, K. Naganuma, H. Itoh, T. Kaino: Third-order nonlinear spectroscopy in As2S3 chalcogenide glass fibers, J. Appl. Phys. **77** (11) 5518 (1995).

[62] P. A. Thielen, L. B. Shaw, P. C. Pureza, V. Q. Nguyen, J. S. Sanghera, I. D. Aggarwal: Small-core As-Se fiber for Raman amplification, Optics Lett. **28** (16) 1406 (2003).

[63] T. Kohoutek, X. Yan, T. W. Shiosaka, S. N. Yannopoulos, A. Chrissanthopoulos, T. Suzuki, Y. Ohishi: Enhanced Raman gain of Ge–Ga–Sb–S chalcogenide glass for highly nonlinear microstructured optical fibers, J. Opt. Soc. Am. B, Vol. , No. () **28** (9) 2285 (2011).

[64] R. E. Slusher, G. Lenz, J. Hodelin, J. Sanghera, L. B. Shaw, I. D. Aggarwal: Large Raman gain and nonlinear phase shifts in high-purity As2Se3 chalcogenide fibers, J. Opt. Soc. Am. B **21** (6) 1147 (2004).

[65] R. R. Alfano, S. L. Shapiro: Emission in the region 4000 to 7000 Å via four-photon coupling in glass, Phys. Rev. Lett. **24** 584 (1970).

[66] R. R. Alfano, S. L. Shapiro: Observation of selfphase modulation and small-scale filaments in crystals and glasses, Phys. Rev. Lett. **24** 592 (1970).

[67] J. C. Knight, T. A. Birks, P. S. J. Russell, D. M. Atkin: All-silica single-mode optical fiber with photonic crystal cladding Opt. Lett. **21** (19) 1547 (1996).

[68] J. M. Dudley, G. Genty, S. Coen: Supercontinuum generation in photonic crystal fiber, Rev. Mod. Phys. **78** (4) 1135 (2006).

[69] X. Jiang, N. Y. Joly, M. A. Finger, F. Babic, G. K. L. Wong, J. C. Travers, P. S. J. Russell: Deep-ultraviolet to mid-infrared supercontinuum generated in solid-core ZBLAN photonic crystal fibre, Nature Photonics **9** 133 (2015).

[70] I. Savelii, J. C. Jules, G. Gadret, B. Kibler, J. Fatome, M. El-Amraoui, N. Manikandan, X. Zheng, F. Désévédavy, J. M. Dudley, J. Troles, L. Brilland, G. Renversez, F. Smektala: Suspended core tellurite glass optical fibers for infrared supercontinuum generation, Optical Materials **33** 1661 (2011).

[71] M. Liao, X. Yan, Z. Duan, T. Suzuki, Y. Ohishi: Tellurite photonic nanostructured fiber, Journal of Lightwave Technology **29** (7) 1018 (2011).

[72] M. Liao, W. Gao, T. Cheng, Z. Duan, X. Xue, T. Suzuki, Y. Ohishi: Flat and broadband supercontinuum generation by four-wave mixing in a highly nonlinear tapered microstructured fiber, Optics Express **20** (26) B574 (2012).

[73] I. Savelii, O. Mouawad, J. Fatome, B. Kibler, F. Désévédavy, G. Gadret, J.-C. Jules, P.-Y. Bony, H. Kawashima, W. Gao, T. Kohoutek, T. Suzuki, Y. Ohishi, F. Smektala: Mid-infrared 2000-nm bandwidth supercontinuum generation in suspended-core microstructured Sulfide and Tellurite optical fibers, Optics Express **20** (24) 27083 (2012).

[74] J. Picot-Clemente, C.Strutynski, F.Amrani, F.Désévédavy, J-CJules, G.Gadret, D. Deng, T.Cheng, K.Nagasaka, Y.Ohishi, B.Kibler, F.Smektala: Enhanced supercontinuum generation in tapered tellurite suspended core fiber, Optics Communications **354** 374 (2015).

[75] P. P. Domachuk, N. A.Wolchover, M. Cronin-Golomb, A. Wang, A. K. George, C. M. B. Cordeiro, J. C. Knight, F. G. Omenetto: Over 4000 nm bandwidth of mid-IR supercontinuum generation in sub-centimeter segments of highly nonlinear tellurite PCFs, Optics Express **16** 7161 (2008).

[76] U. Møller, Y. Yu, I. Kubat, C. R. Petersen, X. Gai, L. Brilland, D. Mechin, C. Caillaud, J. Troles, B. Luther-Davies, O. Bang: Multi-milliwatt mid-infrared supercontinuum generation in a suspended core chalcogenide fiber, Opt. Express **23** (3) 3282 (2015).

[77] M. Boivin, M. El-Amraoui, Y. Ledemi, S. Morency, R. Vallee, Y. Messaddeq: Germanate-tellurite composite fibers with a high-contrast step-index design for nonlinear applications, Optical Materials Express **4** (8) 1740 (2014).

[78] C. R. Petersen, U. Møller, I. Kubat, B. Zhou, S. Dupont, J. Ramsay, T. Benson, S. Sujecki, N. Abdel-Moneim, Z. Tang, D. Furniss, A. Seddon, O. Bang: Mid-infrared supercontinuum covering the 1.4–13.3 μm molecular fingerprint region using ultra-high NA chalcogenide step-index fibre, Nature Photonics **8** 830 (2014).

[79] V. N. Denisov, B. N. Mavrin, V. B. Podobedov: Hyper-Raman scattering by vibrational excitation in crystals, glasses and liquids, PHYSICS REPORTS **151** (1) 1 (1987).

[80] V. Rodriguez: New structural and vibrational opportunities combining Hyper-Rayleigh/hyper-Raman and Raman scattering in isotropic materials, Journal of Raman Spectroscopy **43** (5) 627 (2012).

[81] P. Guyot-Sionnest, Y. R. Shen: Bulk contribution in surface second-harmonic generation, Phys. Rev. B **38** (12) 7985 (1988).

[82] X. Wang, S. Fardad, S. Das, A. Salandrino, R. Hui: Polarization-based identification of bulk contributions in surface nonlinear optics, Phys. Rev. B **93** 161109 (2016).

[83] F. J. Rodríguez, F. X. Wang, B. K. Canfield, S. Cattaneo, M. Kauranen: Multipolar tensor analysis of second-order nonlinear optical response of surface and bulk of glass, Optics Express **15** (14) 8695 (2007).

[84] Y. Sasaki, Y. Ohmori: Phase-matched sum-frequency light generation in optical fibers, Appl. Phys. Lett. **39** (6) 466 (1981).

[85] R. A. Myers, N. Mukherjee, S. R. J. Brueck: Large second-order nonlinearity in poled fused silica, Opt. Lett. **16** (22) 1732 (1991).

[86] A. Okada, K. Ishii, K. Mito, K. Sasaki: Phase-matched second-harmonic generation in novel corona poled glass waveguides, Appl. Phys. Lett. **60** 2853. (1992).

[87] P. G. Kazansky, A. Kamal, P. S. Russell: High second-order nonlinearities induced in lead silicate glass by electron-beam irradiation, Opt. Lett. **18** 683 (1993).

[88] L. J. Henry, B. V. McGrath, T. G. Alley, J. J. Kester: Optical nonlinearity in fused silica by proton implantation, JOSA B **13** 827 (1996).

[89] U. Österberg, W. Margulis: Dye laser pumped by Nd:YAG laser pulses frequency doubled in a glass optical fiber, Opt. Lett. **11** (8) 516 (1986).

[90] R. H. Stolen, H. W. K. Tom: Self-organized phase-matched harmonic generation in optical fibers, Opt. Lett. **12** 585 (1987).

[91] F. Ouellette, K. O. Hill, D. C. Johnson: Light-induced erasure of self-organized $\chi(2)$ gratings in optical fibers, Opt. Lett. **13** (6) 515 (1988).

[92] V. Mizrahi, Y. Hibino, G. Stegeman: Polarization study of photoinduced second-harmonic generation in glass optical fibers, Opt. Commun. **78** 283 (1990).

[93] T. J. Driscoll, N. M. Lawandy: Optically encoded second-harmonic generation in bulk silica-based glasses, Journal of the Optical Society of America B **11** (2) 355 (1994).

[94] W. Margulis, F. Laurell, B. Lesche: Imaging the non linear grating in frequency doubling fibres, Nature **378** (14) 699 (1995).

[95] J. H. Kyung, N. M. Lawandy: Direct measurement of photoinduced charge distribution responsible for second-harmonic generation in glasses, Opt. Lett. **21** (3) 186 (1996).

[96] T. Komatsu: Design and control of crystallization in oxide glasses, Journal of Non-Crystalline Solids **428** 156 (2015).

[97] X. He, C. Fan, B. Poumellec, Q. Liu, H. Zeng, F. Brisset, G. Chen, X. Zhao, M. Lancry: Size-Controlled Oriented Crystallization in SiO2-Based Glasses by Femtosecond Laser Irradiation, Journal of the Optical Society of America B **31** 376 (2014).

[98] A. Stone, H. Jain, V. Dierolf, M. Sakakura, Y. Shimotsuma, K. Miura, K. Hirao, J. Lapointe, R. Kashyap: Direct Laser-Writing of Ferroelectric Single-Crystal Waveguide Architectures in Glass for 3D Integrated Optics, Scientific Reports **5** 10391 (2015).

[99] J. Cao, B. Poumellec, F. Brisset, A.-L. Helbert, M. Lancry: Angular Dependence of the Second Harmonic Generation Induced by Femtosecond Laser Irradiation in Silica-Based glasses: Variation with Writing Speed and Pulse Energy, World Journal of Nano Science and Engineering **5** 96 (2015).

[100] M. B. J. Choi, A. Royon, K. Bourhis, G. Papon, T. Cardinal, L. Canioni, M. Richardson: Three dimensional direct femtosecond laser writing of second-order nonlinearities in glass, Opt. Lett. **37** 1029 (2012).

[101] G. Papon, N. Marquestaut, Y. Petit, A. Royon, M. Dussauze, V. Rodriguez, T. Cardinal, L. Canioni: Femtosecond single-beam direct laser poling of stable and efficient second-order nonlinear optical properties in glass, J. Appl. Phys. **115** (11) 113103 (2014).

[102] G. Papon, Y. Petit, N. Marquestaut, A. Royon, M. Dussauze, V. Rodriguez, T. Cardinal, L. Canioni: Fluorescence and second-harmonic generation correlative microscopy to probe space charge separation and silver cluster stabilization during direct laser writing in a tailored silver containing glass, , , Optical Materials Express **3** (11) 1855 (2013).

[103] N. Mukherjee, R. A. Myers, S. R. J. Brueck: Dynamics of second-harmonic generation in fused silica, J. Opt. Soc. Am. B **11** 665 (1994).

[104] P. G. Kazansky, P. S. J. Russel: Thermally poled glass: frozen-in electric field or oriented dipoles?, Optics Communications **110** 611 (1994).

[105] T. G. Alley, S. R. J. Brueck, M. Wiedenbeck: Secondary ion mass spectrometry study of space-charge formation in thermally poled fused silica, J. Appl. Phys. **86** (12) 6634 (1999).

[106] A. L. C. Triques, I. C. S. Caralho, M. F. Moreira, H. R. Carvalho, R. Fischer, B. Lesche, W. Margullis: Time evolution of depletion region in poled silica, Appl. Phys. Letter, 82 (18), (2003), 2948 **82** (18) 2948 (2003).

[107] F. S. V. Pruneri, G. Bonfrate, P. G. Kazansky, G. M. Yang: Thermal poling of silica in air and under vacuum: The influence of charge transport on second harmonic generation, Appl. Phys. Lett. **74** (17) 2423 (1999).

[108] L. X. X. Jianhua, C. Hongbing, L. Liying, W. Wencheng, Z. congshan, G. Fuxi, : Second harmonic generation investigation on electric poling effects in fused silica, Optical Materials **8** 243 (1997).

[109] E. S. Q. Mingxin, H. Keiichi, M. Toru: The thickness evolution of the second-order nonlinear layer in thermally poled fused silica, Optics Communications **189** 161 (2001).

[110] D. Faccio, V. Pruneri, P. G. Kazansky: Dynamics of the second-order nonlinearity in thermally poled silica glass, Appl. Phys. Lett. **79** (17) 2687 (2001).

[111] A. Kudlinski, Y. Quiquempois, M. Lelek, H. Zeghlache, G. Martinelli: Complete characterization of the nonlinear spatial distribution induced in poled silica glass with a submicron resolution, Appl. Phys. Lett. **83** (17) 3623 (2003).

[112] Y. Quiquempois, N. Godbout, S. Lacroix: Model of charge migration during thermal poling in silica glasses: Evidence of a voltage threshold for the onset of a second-order nonlinearity, Physical Review A **65** (4) (2002).

[113] T. M. Proctor, P. M. Sutton: Static Space-Charge Distributions with a Single Mobile Charge Carrier, The Journal of Chemical Physics **30** (1) 212 (1959).

[114] G. M. Y. Quiquempois, P. Dutherage, P. Bernage, P. Niay, and M. Douay: Localisation of the Induced Second-Order non-Linearity Within Infrasil and Suprasil Thermally Poled Glasses, Opt. Comm. **176** 479 (2000).

[115] M. Dussauze, T. Cremoux, F. Adamietz, V. Rodriguez, E. Fargin, G. Yang, T. Cardinal: Thermal Poling of Optical Glasses: Mechanisms and Second-Order Optical Properties, Int. J. Appl. Glass Sci. **3** (4) 309 (2012).

[116] H. C. S. Chao, Y. Yang, Z. Wang, C. T'sung Shih, H. Niu: "Quasi-Phase-Matched Second-Harmonic Generation in Ge-ion Implanted Fused Silica Channel Waveguide, Optics Express **13** 7091 (2005).

[117] K. A. W. G. Li, A. A. Said, M. Dugan, and P. Bado: Quasi-Phase Matched Second-Harmonic Generation Through Thermal Poling in Femtosecond Laser-Written Glass Waveguides, Optics Express **17** 9442 (2009).

[118] R. J. J. Fage-Pedersen, M. Kristensen: Planar Glass Devices for Efficient Periodic Poling, Opt. Express **13** 8514 (2005).

[119] R. J. J. Fage-Pedersen, M. Kristensen: Poled-Glass Devices: Influence of Surfaces and Interfaces, J. Opt. Soc. Am. B **24** 1075 (2007).

[120] V. Pruneri, G. Bonfrate, P. G. Kazansky, D. J. Richardson, N. G. Broderick, J. P. d. Sandro, C. Simonneau, P. Vidakovic, J. A. Levenson: Greater Than 20%-Efficient Frequency Doubling of v 1532-nm Nanosecond Pulses in Quasi-Phase-Matched germanosilicate Optical Fibers, Opt. Lett. **24** 208 (1999).

[121] A. Strauß, U. Jauernig, V. Reichel, H. Bartelt: Generation of green light in a thermally poled silica fiber by quasi-phase-matched second harmonic generation, Optik - International Journal for Light and Electron Optics **121** (5) 490 (2010).

[122] M. Fokine, L. E. Nilsson, Å. Claesson, D. Berlemont, L. Kjellberg, L. Krummenacher, W. Margulis: Integrated fiber Mach–Zehnder interferometer for electro-optic switching, Opt. Lett. **27** 1643 (2002).

[123] N. Myren, W. Margulis: All-Fiber Electrooptical Mode-Locking and Tuning, IEEE Photonics Technol. Lett. **17** (2047) (2005).

[124] H. An, S. Fleming: Investigating the effectiveness of thermally poling optical fibers with various internal electrode configurations, Optics Express **20** (7) 7436 (2012).

[125] W. Margulis, O. Tarasenko, N. Myren: Who Needs a Cathode? Creating a Second-Order Nonlinearity by Charging Glass Fiber With two Anodes, Opt. Express **17** 15534 (2009).

[126] J. Zhang, Li Qian: Real-time $\chi(2)$ evolution in twin-hole fiber during thermal poling and repoling, JOSA B **26** (7) 1412 (2009).

[127] A. Camara, O. Tarasenko, W. Margulis: Study of thermally poled fibers with a two-dimensional model, Opt Express **22** (15) 17700 (2014).

[128] W. Margulis, Z. Yu, M. Malmström, P. Rugeland, H. Knape, O. Tarasenko: High-speed electrical switching in optical fibers, Applied Optics **50** (25) E65 (2011).

[129] K. W. H. D. E. Carlson, and G. F. Stockdale, : Electrode "Polarization" in Alkali-Containing Glasses, J. Am. Ceram. Soc. **55** 337 (1972).

[130] D. E. Carlson: Ion Depletion of Glass at a Blocking Anode: I, Theory and Experimental Results for Alkali Silicate Glasses, J. Am. Ceram. Soc. **57** 291 (1974).

[131] D. E. Carlson, K. W. Hang, G. F. Stockdale: Ion Depletion of Glass at a Blocking Anode: II, Properties of Ion-Depleted Glasses, J. Am. Ceram. Soc. **57** 295 (1974).

[132] D. E. Carlson: Anodic Proton Injection in Glasses, J. Am. Ceram. Soc. **57** 461 (1974).

[133] F. C. Garcia, I. C. S. Carvalho, E. Hering, W. Margulis, B. Lesche: Inducing a Large Second-Order Optical Nonlinearity in Soft Glasses by Poling, Appl. Phys. Lett. **72** 3252 (1998).

[134] H. An, S. Fleming: Near-anode phase separation in thermally poled soda lime glass, Appl. Phys. Lett. **88** (18) 181106 (2006).

[135] H. An, S. Fleming: Second-order optical nonlinearity in thermally poled borosilicate glass, Appl. Phys. Lett. **89** (18) 181111 (2006).

[136] A. Malakho, M. Dussauze, E. Fargin, O. Bidault, V. Rodriguez, F. Adamietz, B. Poumellec: Effect of sodium to barium substitution on the space charge implementation in thermally poled glasses for nonlinear optical applications, J. Solid State Chem. **182** (5) 1156 (2009).

[137] P. Thamboon, D. M. Krol: Second-order optical nonlinearities in thermally poled phosphate glasses, J. Appl. Phys. **93** (1) 32 (2003).

[138] G. Guimbretière, M. Dussauze, V. Rodriguez, E. I. Kamitsos: Correlation between second-order optical response and structure in thermally poled sodium niobium-germanate glass, Appl. Phys. Lett. **97** (17) 171103 (2010).

[139] M. Dussauze, V. Rodriguez, L. Velli, C. P. E. Varsamis, E. I. Kamitsos: Polarization mechanisms and structural rearrangements in thermally poled sodium-alumino phosphate glasses, J. Appl. Phys. **107** (4) 043505 (2010).

[140] C. R. Mariappan, B. Roling: Mechanism and kinetics of Na+ ion depletion under the anode during electro-thermal poling of a bioactive glass, Journal of Non-Crystalline Solids **356** (11-17) 720 (2010).

[141] M. Dussauze, E. Fargin, M. Lahaye, V. Rodriguez, F. Adamietz: Large Second-Harmonic Generation of Thermally Poled Sodium Borophosphate Glasses, Opt. Express **13** 4064 (2005).

[142] M. Dussauze, E. I. Kamitsos, E. Fargin, V. Rodriguez: Structural Rearrangements and Second-Order Optical Response in the Space Charge Layer of Thermally Poled Sodium-Niobium Borophosphate Glasses, J. Phys. Chem. C **111** 14560 (2007).

[143] E. C. Ziemath, V. D. Araújo, C. A. Escanhoela: Compositional and structural changes at the anodic surface of thermally poled soda-lime float glass, J. Appl. Phys. **104** (5) 054912 (2008).

[144] D. Moncke, M. Dussauze, E. I. Kamitsos, C. P. E. Varsamis: Thermal Poling Induced Structural Changes in Sodium Borosilicate Glasses, Phys. Chem. Glasses **50** (3) 229 (2009).

[145] M. Dussauze, V. Rodriguez, A. Lipovskii, M. Petrov, C. Smith, K. Richardson, T. Cardinal, E. Fargin, E. I. Kamitsos: How Does Thermal Poling Affect the Structure of Soda-Lime Glass?, J. Phys. Chem. C **114** 12754 (2010).

[146] M. Fabbriz, J. R. Senna: Models of Ionic Transport for Silicon-Glass Anodic Bonding, J. Electrochem. Soc. **155** G274 (2008).

[147] P. Nitzsche, K. Lange, B. Schmidt, S. Grigull, U. Kreissig, B. Thomas, K. Herzog: Ion Drift Processes in Pyrex-Type Alkali-Borosilicate Glass During Anodic Bonding, J. Electro. Chem. Soc. **145** 1755 (1998).

[148] B. S. B. Schmidt, P. Nitzsche, K. Lange, S. Grigull, U. Kreissig, B. Thomas, K. Herzog: In Situ Investigation of ion Drift Processes in Glass During Anodic Bonding, Sens. Actuators A **67** 191 (1998).

[149] U. K. Krieger, W. A. Lanford: Field Assisted Transport of Na+ Ions, Ca2+ Ions and Electrons in Commercial Soda-Lime Glass I: Experimental, J. Non-Cryst. Solids **102** 50 (1988).

[150] C. Corbari, L. C. Ajitdoss, I. C. S. Carvalho, O. Deparis, F. P. Mezzapesa, P. G. Kazansky, K. Sakaguchi: The problem of achieving high second-order nonlinearities in glasses: The role of electronic conductivity in poling of high index glasses, Journal of Non-Crystalline Solids **356** (50-51) 2742 (2010).

[151] J. Zakel, M. Balabajew, B. Roling: On the mechanism of field-induced mixed ionic–electronic transport during electro-thermal poling of a bioactive sodium–calcium phosphosilicate glass, Solid State Ionics **265** 1 (2014).

[152] C. McLaren, M. Balabajew, M. Gellert, B. Roling, H. Jain: Depletion Layer Formation in Alkali Silicate Glasses by Electro-Thermal Poling, Journal of The Electrochemical Society **163** (9) H809 (2016).

[153] T. Cremoux, M. Dussauze, E. Fargin, T. Cardinal, D. Talaga, F. Adamietz, V. Rodriguez: Trapped Molecular and Ionic Species in Poled Borosilicate Glasses: Toward a Rationalized Description of Thermal Poling in Glasses, J. Phys. Chem C **118** (7) 3716 (2014).

[154] A. V. Redkov, V. G. Melehin, A. A. Lipovskii: How Does Thermal Poling Produce Interstitial Molecular Oxygen in Silicate Glasses?, J. Phys. Chem C **119** (30) 17298 (2015).

[155] T. Suzuki, J. Anzai, Y. Takimoto, K. Uraji, K. Yamamoto, J. Nishii: Migration behavior of network-modifier cations at glass surface during electrical poling, Journal of Non-Crystalline Solids **452** 125 (2016).

[156] H. Takagi, S.-i. Miyazawa, M. Takahashi, R. Maeda: Electrostatic Imprint Process for Glass, Appl. Phys. Expr. **1** 024003 (2008).

[157] P. Brunkov, V. Goncharov, V. Melehin, A. Lipovskii, M. Petrov: Submicron Surface Relief Formation Using Thermal Poling of Glasses, E-j. surf. sci. nanotechnol. **7** 617 (2009).

[158] A. Abdolvand, A. Podlipensky, S. Matthias, F. Syrowatka, U. Gösele, G. Seifert, H. Graener: Metallodielectric Two-Dimensional Photonic Structures Made by Electric-Field Microstructuring of Nanocomposite Glasses, Advanced Materials **17** (24) 2983 (2005).

[159] A. A. Lipovskii, V. V. Rusan, D. K. Tagantsev: Imprinting phase/amplitude patterns in glasses with thermal poling, Solid State Ionics **181** (17-18) 849 (2010).

[160] A. V. Redkov, V. V. Zhurikhina, A. A. Lipovskii: Formation and self-arrangement of silver nanoparticles in glass via annealing in hydrogen: The model, Journal of Non-Crystalline Solids **376** 152 (2013).

[161] A. N. Kamenskii, I. V. Reduto, V. D. Petrikov, A. A. Lipovskii: Effective diffraction gratings via acidic etching of thermally poled glass, Optical Materials **62** 250 (2016).

[162] L. A. H. Fleming, D. M. Goldie, A. Abdolvand: Imprinting of glass, Optical Materials Express **5** (8) 1674 (2015).

[163] P. N. Brunkov, V. G. Melekhin, V. V. Goncharov, A. A. Lipovskii, M. I. Petrov: Submicron-resolved relief formation in poled glasses and glass-metal nanocomposites, Tech. Phys. Lett. **34** (12) 1030 (2008).

[164] G. Yang, M. Dussauze, V. Rodriguez, F. Adamietz, N. Marquestaut, K. L. N. Deepak, D. Grojo, O. Uteza, P. Delaporte, T. Cardinal, E. Fargin: Large scale micro-structured optical second harmonic generation response imprinted on glass surface by thermal poling, J. Appl. Phys. **118** (4) 043105 (2015).

[165] V. R. M. Dussauze, F. Adamietz, G.Yang, F. Bondu, A. Lepicard, M. Chafer, T. Cardinal, E. Fargin: Accurate Second Harmonic Generation Microimprinting in Glassy Oxide Materials, Advanced Optical Materials **4** (6) 929 (2016).

[166] K. Sokolov, V. Melehin, M. Petrov, V. Zhurikhina, A. Lipovskii: Spatially periodical poling of silica glass, J. Appl. Phys. **111** (10) 104307 (2012).

[167] H. Nasu, K. Kubodera, M. Kobayashi, M. nakamura, K. Kamiya: 3rd-harmonic generation from some chalcogenide glasses, Journal of the American Ceramic Society **73** (6) 1794 (1990).

[168] M. Asobe, T. Kanamori, K. Kubodera: Ultrafast All-Optical Switching Using Highly Nonlinear Chalcogenide Glass-Fiber., IEEE Photonics Technology Letters **4** (4) 362 (1992).

[169] F. Smektala, C. Quemard: Chalcogenide glasses with large non-linear refractive indices., Journal of Non-Crystalline Solids **239** (1-3) 139 (1998).

[170] K. Ogusu, J. Yamasaki, S. Maeda, M. Kitao, M. Minakata: Linear and nonlinear optical properties of Ag-As-Se chalcogenide glasses for all-optical switching, Opt. Lett. **29** (3) 265 (2004).

[171] D. I. Yeom, E. C. Maegi, M. R. E. Lamont, M. A. F. Roelens, L. Fu, B. J. Eggleton: Low-threshold supercontinuum generation in highly nonlinear chalcogenide nanowires, Opt. Lett. **33** (7) 660 (2008).

[172] M. Guignard, V. Nazabal, F. Smektala, J. L. Adam, O. Bohnke, C. Duverger, A. Moréac, H. Zeghlache, A. Kudlinski, G. Martinelli, Y. Quiquempois: Chalcogenide Glasses Based on Germanium Disulfide for Second Harmonic Generation, Advanced Functional Materials **17** (16) 3284 (2007).

[173] W. Liu, Q. M. Zhang, L. Liu, L. Xu, Y. Xu, G. Chen: Enhancement of second-order optical nonlinearity in photo-darkened Ge25Sb10S65 chalcogenide glass by femtosecond laser light, Optics Communications **282** (10) 2081 (2009).

[174] R. Jing, Y. Guang, Z. Huidan, C. Guorong, K. Tanaka, K. Fujita, S. Murai, Y. Tsujiie: Second-harmonic generation in thermally poled chalcohalide glass, Opt. Lett. **31** (23) 3492 (2006).

[175] G. Dong, H. Tao, X. Xiao, C. Lin, X. Zhao, S. Mao: Mechanism of electron beam poled SHG in 0.95GeS2·0.05In2S3 chalcogenide glasses, Journal of Physics and Chemistry of Solids **68** (2) 158 (2007).

[176] H. Zeghlache, M. Guignard, A. Kudlinski, Y. Quiquempois, G. Martinelli, V. Nazabal, F. Smektala: Stabilization of the second-order susceptibility induced in a sulfide chalcogenide glass by thermal poling, J. Appl. Phys. **101** (8) 084905 (2007).

[177] S. Gu, Z. Ma, H. Tao, C. Lin, H. Hu, X. Zhao, Y. Gong: Second-harmonic generation in the thermal/electrical poling (100-x)GeS2·x(0.5Ga2S3·0.5CdS) chalcogenide glasses, Journal of Physics and Chemistry of Solids **69** (1) 97 (2008).

[178] A. V. Y. Quiquempois, D. Dam, K. Turcotte, J. Maier, G. Stegeman S. Lacroix: Second-order nonlinear susceptibility in As2S3 chalcogenide thin glass films, Electronics letters **36** (8) 733 (2000).

[179] W. T. Shoulders, J. Novak, M. Dussauze, J. D. Musgraves, K. Richardson: Thermal poling behavior and SHG stability in arsenic-germanium sulfide glasses, Optical Materials Express **3** (6) 700 (2013).

[180] M. Dussauze, X. Zheng, V. Rodriguez, E. Fargin, T. Cardinal, F. Smektala: Photosensitivity and second harmonic generation in chalcogenide arsenic sulfide poled glasses, Optical Materials Express **2** (1) 45 (2012).

[181] K. Shimakawa, S. Inami, S. R. Elliott: Reversible photoinduced change of photoconductivity in amorphous chalcogenide films, Physical Review B **42** (18) 11857 (1990).

[182] K. Shimakawa, S. Inami, T. Kato, S. R. Elliott: Origin of photoinduced metastable defects in amorphous chalcogenides, Physical review B **46** (16) 10062 (1992).